



Norwegian University of  
Science and Technology

# Long-Term Properties of Interlaminar Shear Strength of Composite Laminates

**Anna Birgitte Monsås**

Master of Science in Mechanical Engineering

Submission date: April 2018

Supervisor: Andreas Echtermeyer, MTP

Norwegian University of Science and Technology  
Department of Mechanical and Industrial Engineering



# Preface and Acknowledgment

The work presented in this report was conducted in the period from October 2017 to April 2018 at Department of Mechanical and Industrial Engineering (MTP) at Norwegian University of Science and Technology (NTNU). The work is part of a Joint Industrial Project called "Affordable Composites" led by DNV GL, and submitted in partial fulfillment of the requirement for the MSc degree at MTP.

I wish to acknowledge Ph.D. student Abedin Gagani for the valuable input and close supervising during the course of the work. I would also like to thank my supervisor Prof. Andreas Echtermeyer for his help and guidance.

Personally, this thesis marks the end of a six-year stay at NTNU. I would like to thank all of the individuals I have met during this period who made the stay unforgettable.

In particular, I want to thank my close friend Marie Kjeldsen Bergvoll who sadly is no longer among us. She inspired me daily, both academically and personally, for five years at the university. Her memory will always be in my heart.

NTNU, Trondheim, 13th April 2018

Anna Monsås



# Abstract

Components made of fiber reinforced polymers (FRP) are frequently used in environments with fluctuating temperatures and moisture levels. These environmental factors lead to a degradation of the FRP in the long term. The mechanisms behind the degradation of FRPs and its effect on mechanical performance are not fully understood. For this reason, the main objective of this master thesis is to study how environmental factors, i.e. water and heat, affect the interlaminar shear strength (ILSS) of FRPs. This was achieved by conducting static and fatigue four-point flexural bending tests on I-beam shaped glass fiber/epoxy specimens. Both dry and conditioned specimens were tested. Conditioned specimens were immersed in a distilled water bath at 60°C for three months prior to testing. The tests were performed at temperatures of 40°C and 60°C. The obtained data was compared to data obtained at room temperature. An increase in test temperature led to a decrease in shear strength, shear modulus and yield strength and an increase in deflection at failure. This was also seen as a result of conditioning. An increase in test temperature led to a shorter fatigue life for the specimens. Conditioning showed similar effects. The degradation in mechanical performance should be considered when designing FRP components intended for use in harsh environments. The results obtained in this study can potentially be used in the development of models aiming to predict long-term properties of FRPs.



## Sammendrag

Komponenter laget av kompositter (fiberforsterkede polymerer) blir ofte brukt i miljøer hvor temperaturen og fuktigheten fluktuerer. Disse miljøfaktorene gjør at kompositten degraderes over tid. Per dags dato finnes det lite kunnskap om hvilke mekanismer som står bak denne degraderingen og hvordan dette påvirker materialets mekaniske egenskaper. I denne masteroppgaven er det derfor undersøkt hvordan vann og endringer i temperatur påvirker skjæregenskapene til kompositter. Dette ble gjort ved å utføre firepunkts bøyestester, både statiske og dynamiske (utmattelse), på prøvestykker formet som H-bjelker. Prøvestykkene var av glassfiber og epoxy. Halvparten av prøvestykkene ble lagt i vann i tre måneder før testing. Resterende prøvestykker ble ikke behandlet i vann før testing. Bøyetestene ble utført ved temperaturer på 40°C og 60°C. Resultatene ble sammenlignet med data innhentet fra bøyestester utført ved romtemperatur. En økning i testtemperatur førte til en lavere skjærstyrke og skjærmodul, og en større nedbøying før prøvestykket ble ødelagt. Det samme kunne sees som et resultat av at prøvestykkene ble behandlet i vann. En økning i testtemperatur førte også til at utmattelseslevetiden til prøvestykkene ble kortere. Vannbehandling av prøvestykkene ga et lignende resultat på utmattingskurvene. Degraderingen av mekaniske egenskaper som et resultat av fuktighet og varme burde bli tatt med i betraktning når en skal designe komposittkomponenter tiltenkt bruk i krevende miljøer. Resultatene innhentet i dette arbeidet kan også brukes i utviklingen av modeller som sikter på å forutse langtidsegenskaper til kompositter.





## Acronyms and Abbreviations

<b>Acr./Abbr.</b>	<b>Description</b>
FEM	Finite Element Modeling
FRP	Fiber Reinforced Plastic or Polymer
HDE	Hysterisis Dissipated Energy
ILSS	Interlaminar Shear Strength
RT	Room Temperature
RVE	Representative Volume Element



# Contents

<b>Preface and Acknowledgment</b>	<b>i</b>
<b>Abstract</b>	<b>iii</b>
<b>Sammendrag</b>	<b>v</b>
<b>Acronyms and Abbreviations</b>	<b>vii</b>
<b>List of Tables</b>	<b>xiii</b>
<b>List of Figures</b>	<b>xv</b>
<b>1 Introduction</b>	<b>1</b>
1.1 Background . . . . .	1
1.2 Objectives . . . . .	2
1.3 Scope . . . . .	2
<b>2 Theory</b>	<b>3</b>
2.1 Composites . . . . .	3
2.1.1 Structure . . . . .	3
2.1.2 Stiffness and strength . . . . .	4
2.2 Water uptake in composites . . . . .	6
2.3 Multiscale approach to predict long-term properties of composites . . . . .	8
2.3.1 Model outline . . . . .	8
2.3.2 Heat and moisture transport . . . . .	8
2.3.3 Degradation of constituents . . . . .	9
2.3.4 Behaviour on the macro level based on the constituent properties . . . . .	10
2.3.5 Prediction of the composite lifetime . . . . .	10
2.3.6 This work's contribution to a multiscale model . . . . .	11
<b>3 Experimental</b>	<b>13</b>
3.1 Material . . . . .	13
3.2 Preparation of the composite laminate . . . . .	13
3.3 Preparation of I-beam specimens . . . . .	14
3.4 Sample conditioning . . . . .	15
3.5 Volume fraction measurement . . . . .	16
3.6 Four-point bending . . . . .	17

3.6.1	General setup . . . . .	17
3.6.2	Static testing . . . . .	21
3.6.3	Fatigue testing . . . . .	21
3.7	Damage analysis . . . . .	22
<b>4</b>	<b>Results</b>	<b>23</b>
4.1	Introductory remarks . . . . .	23
4.2	Water uptake . . . . .	23
4.2.1	Analytical model . . . . .	23
4.2.2	Experimental . . . . .	25
4.3	Static behavior . . . . .	27
4.3.1	Main results . . . . .	27
4.3.2	Comparison of laminate A and B . . . . .	31
4.3.3	Static tests of beams immersed in water for one year . . . . .	32
4.4	Fatigue behaviour . . . . .	33
4.4.1	Introductory remarks . . . . .	33
4.4.2	Fatigue life . . . . .	33
4.4.3	Damage analysis . . . . .	35
4.4.4	Deflection during fatigue testing . . . . .	37
4.4.5	Hysterisis loops, dissipated energy and stiffness evolution . . . . .	38
<b>5</b>	<b>Discussion</b>	<b>41</b>
5.1	Discrepancy in water uptake . . . . .	41
5.2	Selecting the right fatigue failure limit . . . . .	42
5.3	Accuracy of test procedure . . . . .	44
5.4	Temperature effects on dry specimens . . . . .	45
5.5	Temperature effects on wet specimens . . . . .	47
5.6	Effects of conditioning . . . . .	48
5.7	Application of results . . . . .	49
<b>6</b>	<b>Conclusions</b>	<b>51</b>
<b>7</b>	<b>References</b>	<b>53</b>
<b>8</b>	<b>Appendix</b>	<b>59</b>
(A)	Task description . . . . .	59
(B)	Data from static tests . . . . .	61
(C)	Data from fatigue tests . . . . .	61
(D)	Light transmittance photos . . . . .	63

(E) Risk assessment . . . . . 64



# List of Tables

- 3.1 Constituent properties of the glass/epoxy laminate used in this work. . . . 13
- 3.2 Overview of the number of static tests performed in this work and what laminate is used for the different tests. . . . . 21
- 3.3 Overview of the number of fatigue tests performed in this work and what laminate is used for the different tests.. . . . 21
- 4.1 Experimentally and analytically obtained shear strength and modulus at room temperature. . . . . 30
- 4.2 Static properties of laminate A and B. . . . . 31
- 4.3 Model parameters and R-squared values from the linear regression of each SN-curve. . . . . 34
- 8.1 Data from static tests executed in this work. . . . . 61
- 8.2 Fatigue life and testing conditions of the dry specimens. . . . . 61
- 8.3 Fatigue life and testing conditions of the wet specimens. . . . . 62





# List of Figures

- 2.1 Constituents in a fiber reinforced polymer. . . . . 3
- 2.2 Shear in unidirectional composites. . . . . 4
- 2.3 Schematic of an anisotropic composite with laminate coordinate system. . . . . 7
- 2.4 Schematic of fatigue curves. . . . . 11
- 3.1 The vacuum bagging system set-up used in this work. . . . . 14
- 3.2 I-beam dimensions, the length of the beams were 60 mm. . . . . 15
- 3.3 I-beam fiber and ply stacking direction. . . . . 16
- 3.4 Schematic showing the distances between rollers. . . . . 17
- 3.5 Anti-buckling device. . . . . 17
- 3.6 Test set-up for dry testing. . . . . 18
- 3.7 Test set-up for wet testing. . . . . 18
- 3.8 Shear force and bending moment diagram of the I-beam. . . . . 19
- 3.9 Shape of shear stress distribution over the beam’s cross-section. . . . . 20
- 3.10 Schematic showing the representative cross-section for micrographs. . . . . 22
- 4.1 Schematic showing the sections for the analytical water uptake solution. . . . . 24
- 4.2 Experimental and analytical water uptake as mass increase versus time of immersion. . . . . 26
- 4.3 The I-beam before and after conditioning. . . . . 26
- 4.4 Shear stress-deflection curves for different environments. . . . . 27
- 4.5 Mean shear strength for different environments. . . . . 28
- 4.6 Mean deflection at failure for different environments. . . . . 28
- 4.7 Mean yield strength for different environments. . . . . 29
- 4.8 Mean shear modulus for different environments. . . . . 30
- 4.9 Stress-deflection curves of samples made from laminate A and B. . . . . 31
- 4.10 Stress-deflection curves of samples conditioned for three months and one year. . . . . 32
- 4.11 Fatigue data and SN-curves for different environments. . . . . 34
- 4.12 Light transmittance photos of specimens subsequent to fatigue testing. . . . . 35
- 4.13 Microscopic observation of damage in the web of the beam’s cross section for the different test environments. . . . . 36
- 4.14 Maximum deflection versus the normalized number of cycles. . . . . 37
- 4.15 Representative hysteresis loops for each test environment. . . . . 39
- 4.16 Fatigue evolution of absolute and normalized hysteresis dissipated energy (HDE). . . . . 40
- 4.17 Fatigue evolution of absolute and normalized secant shear modulus. . . . . 40

5.1	SN-curves with different fatigue failure deflection limits. . . . .	42
5.2	Schematic illustrating regions in fatigue testing, adapted from [1]. . . . .	43
5.3	SN-curves with different fatigue failure limits. . . . .	43
5.4	Comparison of static shear strength, $\tau_{max}$ , and parameter from fatigue curve regression, $\tau_0$ . . . . .	46
5.5	Comparison of static shear modulus, $G_{12}$ , and slope of SN-curve, $-1/k$ . . .	46
8.1	Light transmittance photos of every specimen tested in fatigue. . . . .	63

# 1 Introduction

## 1.1 Background

Offshore components are exposed to harsh environmental factors such as sea water and fluctuating temperatures. A problem with traditional engineering materials, i.e. metals, is that they are vulnerable to corrosion in offshore and marine environments [2]. Fiber reinforced polymers (FRPs) are a promising alternative to metals due to their corrosion resistance [3]. In addition, FRPs are easy to tailor and have a high stiffness and strength to mass ratio [4]. Due to these excellent material properties, the use of FRPs has increased over the last years [5, 2, 6]. A problem with FRPs is that they degrade in the long term in contact with the above-mentioned environmental factors, especially in combination with fluctuating loads [7]. Despite the fact that this has been a research topic for many years, the mechanisms behind the environmental degradation of FRPs, and what they do to the mechanical performance of FRPs, are not fully understood [7, 6, 8]. As a result, it is not possible to accurately predict how FRPs behave in the long term when they are exposed to different environmental factors.

It is especially important to increase the understanding of the long-term behavior of the FRP's interlaminar shear strength (ILSS). ILSS is an important design factor to consider when employing laminated composites, i.e. FRPs, in structural applications. Composites are often joined with other components, such as metal parts, where shear becomes the main transferring load [2]. This is the reason to why the long-term environmental effect on ILSS is important to test.

A commonly used method to test how environmental factors affect ILSS is to immerse short-beam specimens in water for a long period of time, called conditioning, and subsequently subjecting them to a short-beam bending test [7, 5, 9]. The water diffuses into the composite specimens until they are thought to saturate. Bringing the material to saturation is desirable as it gives the best basis to identify long-term behavior. The conditioning process can be time-consuming and is highly dependent on the thickness of the specimen in the diffusion direction. Therefore, Gagani et al. suggested to test novel I-beam specimens with a thin cross-section, allowing the beams to saturate quickly [10]. Testing short I-beams in a four-point bending fixture at different test temperatures would give valuable information about the environmental effect on ILSS.

## 1.2 Objectives

This thesis is part of a Joint Industrial Project (JIP) called "Affordable Composites" led by DNV GL. The JIP investigates long-term properties of composites and how they can be predicted by using material mathematical modeling. The main objective of this specific thesis is to study how environmental factors, i.e. water and heat, affect ILSS of glass fiber/epoxy composites.

## 1.3 Scope

Four-point flexural bending tests are conducted to analyze the static and fatigue behavior of the material's ILSS. The specimens have an I-beam shape. Both dry and conditioned specimens are tested. Conditioned specimens were immersed in a distilled water bath at 60°C for three months prior to testing. The tests were performed at temperatures of 40°C and 60°C and compared to data obtained at room temperature by Gagani et al. [10]. The damage in the specimens was analyzed using an optical microscope. A formal task description is given at the beginning of the Appendix.

## 2 Theory

### 2.1 Composites

#### 2.1.1 Structure

Composites are materials consisting of two or more constituents with distinct differences in properties on a scale higher than the molecular scale [3]. Fiber reinforced polymers (FRPs) are some of the most commonly used types of composites. The fibers can be arranged in various ways, such as randomly distributed, woven or laid up in parallel and they may have different lengths [11]. An FRP with long, parallel fibers is referred to as a unidirectional continuous-fiber-reinforced polymer, and its microstructure is illustrated in figure 2.1. The polymer is referred to as the matrix, while the region between the fiber and the matrix is referred to as the interface. The fibers are usually treated with a chemical mixture called sizing. The sizing ensures satisfying adherence between the fibers and the matrix, and contributes to the behavior of the interface [3]. The behavior of a composite is highly dependent on the properties of its constituents in addition to the fiber volume fraction. The fiber volume fraction is defined as the volume of fibers over the total volume of the composite. Moreover, structural defects such as voids influence the behavior of the material.

The composite studied in this work is made of glass fibers and epoxy, two commonly used constituents [11]. No other fiber matrix system will be discussed in this thesis.

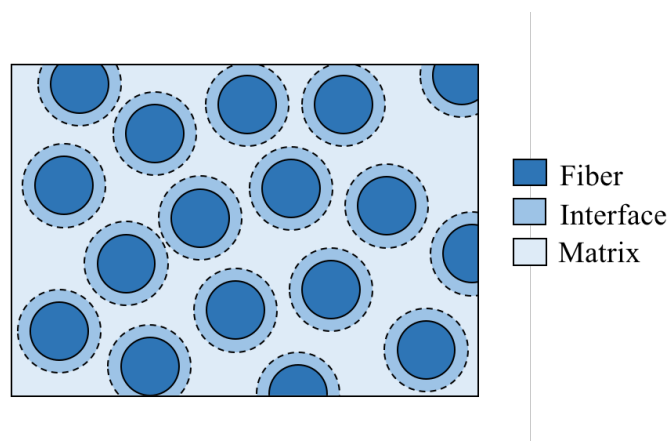


Figure 2.1: Constituents in a fiber reinforced polymer.

### 2.1.2 Stiffness and strength

A micromechanical model calculates the macromechanical properties of a composite using the properties and allocation of its constituent materials [4]. The simplest and most well-known micromechanical model is the rule of mixture, which estimates the fibrous composite's elastic modulus as [3]

$$E = E_f V_f + E_m (1 - V_f) \quad (2.1)$$

where  $E_f$  and  $E_m$  are tensile moduli of the fiber and the matrix, respectively.  $V_f$  is the fiber volume fraction.

Numerous micromechanical models predicting elastic properties of composites have been developed over the years, while it has been shown to be more intricate to develop models predicting the strength of composites [12]. Consequently, fewer models have been proposed in the literature. In 1998, Hinton and Soden addressed this problem by organizing a comprehensive coordinating study to describe, compare and verify some of the most known failure theories until that date [13, 14]. One theory that performed well in the study was described by Chamis et al. [15, 16]. Chamis' theory covers a wide range of macromechanical properties, including ILSS. The equation for calculating the ILSS of a unidirectional continuous-fiber-reinforced polymer is given by Chamis et al. as

$$\tau_{max} = [1 - (\sqrt{V_f} - V_f)(1 - \frac{G_m}{G_{f12}})]\tau_{max}^m \quad (2.2)$$

where  $V_f$  is the fiber volume fraction,  $G_m$  is the shear modulus of the matrix,  $G_{f12}$  is the longitudinal shear modulus of the fiber and  $\tau_{max}^m$  is the shear strength of the matrix. The shear strength is illustrated in figure 2.2.

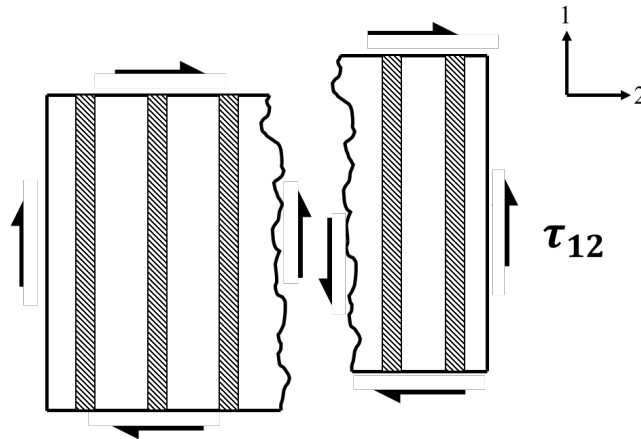


Figure 2.2: Shear in unidirectional composites.

Furthermore, Chamis et al. suggested an equation predicting the shear modulus, given as

$$G_{12} = \frac{G_m}{1 - \sqrt{V_f}(1 - G_m/G_{f12})} \quad (2.3)$$

where the parameters are the same as in equation 2.2.

The Bridging Model proposed by Huang et al. is another micromechanical theory mentioned in Hinton and Soden's study [4, 17]. Huang's in-plane shear strength equation is given as

$$\tau_{max} = \min\left\{\frac{\sigma_U^f - (\alpha_e^f - \alpha_p^f)\sigma^0}{\alpha_p^f}, \frac{\sigma_U^m - (\alpha_e^m - \alpha_p^m)\sigma^0}{\alpha_p^m}\right\} \quad (2.4)$$

where

$$\sigma^0 = \min\left\{\frac{\sigma_Y^m}{\sqrt{3}\alpha_e^m}, \frac{\sigma_U^f}{\alpha_e^f}\right\} \quad (2.5)$$

$$\alpha_e^f = \frac{G_{f12}}{V_f G_{f12} + 0.5(1 - V_f)(G_m + G_{f12})} \quad (2.6)$$

$$\alpha_e^m = \frac{0.5(G_{f12} + G_m)}{V_f G_{f12} + 0.5(1 - V_f)(G_m + G_{f12})} \quad (2.7)$$

$$\alpha_p^f = \frac{3G_{f12}}{3V_f G_{f12} + 0.5(1 - V_f)(E_T^m + 3G_{f12})} \quad (2.8)$$

$$\alpha_p^m = \frac{0.5(3G_{f12} + E_T^m)}{3V_f G_{f12} + 0.5(1 - V_f)(E_T^m + 3G_{f12})} \quad (2.9)$$

where  $\sigma_U^f$  is the tensile strength of the fiber.  $\sigma_Y^m$  and  $\sigma_U^m$  are the yield and ultimate tensile strength of the matrix, respectively.  $E_T^m$  is the hardening modulus of the matrix. Huang also proposed a shear modulus equation, given as [17]

$$G_{12} = \frac{(G_{f12} + G_m) + V_f(G_{f12} - G_m)}{(G_{f12} + G_m) - V_f(G_{f12} - G_m)} G_m \quad (2.10)$$

## 2.2 Water uptake in composites

Composites absorb moisture when exposed to humid environments. Water molecules from the environment diffuse into the material, and the amount of water present in the composite increases with time when being continuously exposed to the humid environment. After a certain amount of time, the water uptake rate decreases and eventually becomes close to zero. At this point, the composite can be defined as saturated. This behavior is often modeled by Fick's law, even though the validity of it is debated [18, 19]. Fick's first law in one dimension describes water diffusion through a section. It is given as [20, 21, 8]

$$F = -D \frac{\partial C}{\partial x} \quad (2.11)$$

where  $F$  is the rate of transfer per unit area of section,  $D$  is the diffusion coefficient,  $C$  is the concentration of water in the composite and  $x$  is the directional constant normal to the section. Fick's law can be written as a differential equation as

$$\frac{\partial C}{\partial t} = D \frac{\partial^2 C}{\partial x^2} \quad (2.12)$$

and is referred to as Fick's second law. By separation of variables, equation 2.12 has the solution [22]

$$C(x, t) = C_{eq} \left[ 1 - \frac{4}{\pi} \sum_{i=0}^{\infty} \frac{(-1)^i}{2i+1} \cos \frac{(2i+1)\pi x}{L} \exp[-(2i+1)^2 \left(\frac{\pi}{L}\right)^2 Dt] \right] \quad (2.13)$$

where  $C_{eq}$  is the concentration of water in the composite when it is saturated and  $t$  is time.  $L$  is the thickness in the diffusion direction. The mass percent of water can be obtained by integrating equation 2.13 over the diffusion length  $L$ ;

$$M(t) = \int_0^L C(x, t) dx \quad (2.14)$$

which yields

$$M(t) = M_{eq} \left[ 1 - \frac{8}{\pi^2} \sum_{i=0}^{\infty} \frac{\exp[-(2i+1)^2 \left(\frac{\pi}{L}\right)^2 Dt]}{(2i+1)^2} \right] \quad (2.15)$$

where  $M_{eq}$  is the mass percent of water in the composite when it is saturated. Note that the water uptake is dependent on the square value of the diffusion length. Hence, the time to reach saturation is highly dependent on the thickness in the diffusion direction.



Often, the diffusion problem at hand is not limited to one dimension. When dealing with diffusion in composites in more than one dimension, the anisotropy of the material must be considered. The diffusivity parallel to the fiber direction,  $D_x$ , is greater than the diffusivity transverse to the fiber direction,  $D_y = D_z$ , see figure 2.3 [23]. Fick's second law in two and three dimensions for an anisotropic material is given as

$$\frac{\partial C}{\partial t} = D_x \frac{\partial^2 C}{\partial x^2} + D_y \frac{\partial^2 C}{\partial y^2} \quad (2.16)$$

and

$$\frac{\partial C}{\partial t} = D_x \frac{\partial^2 C}{\partial x^2} + D_y \frac{\partial^2 C}{\partial y^2} + D_z \frac{\partial^2 C}{\partial z^2} \quad (2.17)$$

respectively. The solution to these equations are given by Blikstad and presented in section 4.2.1 [22].

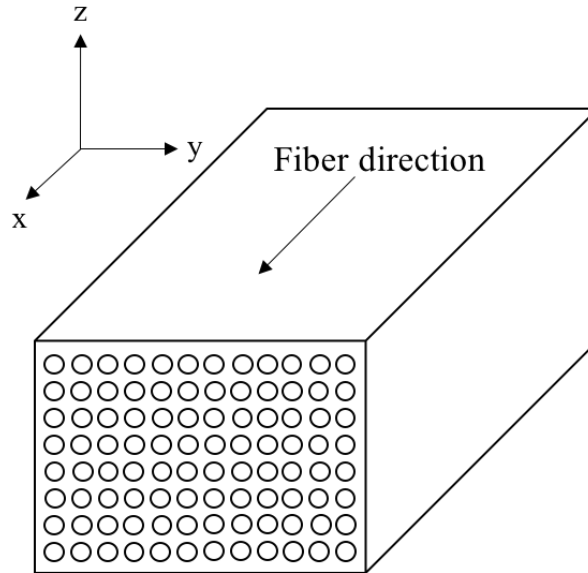


Figure 2.3: Schematic of an anisotropic composite with laminate coordinate system.

## **2.3 Multiscale approach to predict long-term properties of composites**

### **2.3.1 Model outline**

Upon writing this thesis, no established method to accurately predict how composites behave in the long term when exposed to different environmental factors exists. As a result, composite components are subjected to time-consuming and expensive tests prior to application. It is desirable to reduce the amount of testing by developing material mathematical models that aim to predict long-term properties of composites. A multiscale analysis approach is the most promising method upon writing this thesis [8]. A multiscale model intended to predict long-term behavior of composites can be comprised of the following steps:

1. Predict heat and moisture transport in the composite
2. Predict how heat and moisture affect the composite's constituent properties on the micro level
3. Predict the composite's properties on a macro level based on its constituent properties
4. Predict the composite's lifetime

Each of these steps is slightly elaborated in the following subsections. Eventually, how the work presented in this thesis contributes to the multiscale model is indicated.

### **2.3.2 Heat and moisture transport**

The constituent properties are dependent on temperature and moisture content within the material. For a multiscale model it is therefore desirable to know the temperature or amount of moisture in the composite as a function of time and position. One way to predict these distributions is to utilize two analogous laws; Fourier's law and Fick's law (as already described in section 2.2) [6]. The governing equation behind these laws can be solved for complex geometries utilizing finite element modeling (FEM) [23, 24]. On the microscale level, heat conductivity and mass diffusivity vary [8]. These variations should be taken into account in a precise heat and moisture transport model. Note that heat equilibrium is reached much faster than moisture equilibrium [3].

### 2.3.3 Degradation of constituents

Water and heat affect the constituents of a composite in different ways. In the matrix and the interface, water molecules diffuse into the material and arrange themselves between the polymer chains which increase the distance between them [25, 26]. This results in an increased chain mobility, thus the water acts as a plasticizer and lowers the modulus of the matrix and interface [24]. The same effect is seen as a result of an increase in temperature within the material [27]. Water molecules, in addition to increasing the chain mobility, results in swelling of the interface and matrix. This effect is reversible, but if the swelling strains become excessive, it can result in microcracking in the matrix and interface and/or fiber matrix debonding [18].

In contrast to the matrix and interface, the most frequently used composite fibers, i.e. glass and carbon, do not absorb moisture [5, 24]. However, it is widely known that the presence of water at the glass fiber surface results in a weakening of the material [28, 3]. The degradation depends on the amount of moisture present at the fiber surface, amount and duration of applied stress, the constituents of the glass material and the presence of surface cracks and other flaws in the fibers [18]. When glass fibers are surrounded by a polymer matrix, water needs to diffuse through the polymer resin before it reaches the fiber. Hence, the polymer matrix is protecting the fiber from direct contact with water and severely reducing the amount of water reaching the fiber surface [8]. If the reinforcing fibers are degraded, the overall performance of the composite may be substantially lowered. This is especially true for the tensile properties in the fiber direction, and less true for shear properties that are matrix-dominated [3]. Regarding heat, glass fibers generally lose their strength when subjected to higher temperatures [3]. However, the temperature level where such changes are seen in the glass fiber is much higher than the upper service temperatures of polymer matrices [29, 30].

How temperature and moisture affect the constituents should be established and included in the multiscale model. It is desirable to include a function with moisture content and temperature as an input, and constituent material property, e.g. modulus, as output. This relation can be found by individually testing the fiber, matrix and interface at different temperatures and moisture contents, and subsequently fitting the experimentally obtained data to adequate curves. Ideally, a more fundamental degradation equation based on theory should be found, such as chemistry and polymer science for the degradation of the matrix and interface [8].

### 2.3.4 Behaviour on the macro level based on the constituent properties

After establishing how the environmental factors affect the constituent properties, it is necessary to find a method that predicts the effective ply properties based on the degraded constituent properties. The simplest methods available are analytical, such as Chamis' and Huang's micromechanical models mentioned in section 2.1.2. Such analytical models are typically not very accurate, and they usually ignore the contribution of the interface [6]. A more promising alternative is the Representative Volume Element (RVE) [8, 6]. The RVE models the fibers, matrix and interfaces separately on a microscale level and representative finite elements are added to these constituent regions. By examining the RVE with FEM, it is possible to determine the homogenized properties of the composite.

### 2.3.5 Prediction of the composite lifetime

It is widely acknowledged that cyclic loading below the materials ultimate strength reduces its lifetime. As cyclic loads are unavoidable in service, it is important to establish the materials fatigue behavior when considering it for an application. Predicting a composite's fatigue behavior is a complex task. According to literature, no model going from constituent properties to fatigue behavior exists [8]. Therefore, fatigue life has to be measured. The lifetime of a material is typically measured by examining how many cycles of a periodically fluctuating load the material can handle until failure. One fatigue test results in one of the data points seen in figure 2.4. When a sufficient number of fatigue tests are performed, the data points are typically interpolated to Basquin's equation [31]

$$\tau = \tau_0 N_f^{-1/k} \quad (2.18)$$

where  $\tau$  is the applied stress (here it is the maximum applied shear stress, but it could also have been amplitude tensile stress, among others).  $\tau_0$  and  $k$  are empirical interpolation constants, and  $N_f$  is the number of cycles until failure.

Fatigue curves are usually measured at room temperature in a standard laboratory atmosphere. When the inspected material is exposed to environmental factors causing a degradation, the measured SN-curve (fatigue curve) has shown to shift downward and experience a change of slope [7, 19, 32], illustrated in figure 2.4. Hence, the material resists fewer load cycles until it fails at a given stress level as a result of degradation. However, research reporting and investigating this phenomenon is quite scarce.

Each SN-curve takes a long time to obtain. In order to reduce the test-time, it would be beneficial to increase the understanding, quantify and potentially predict environmental effects on composites' fatigue behavior.

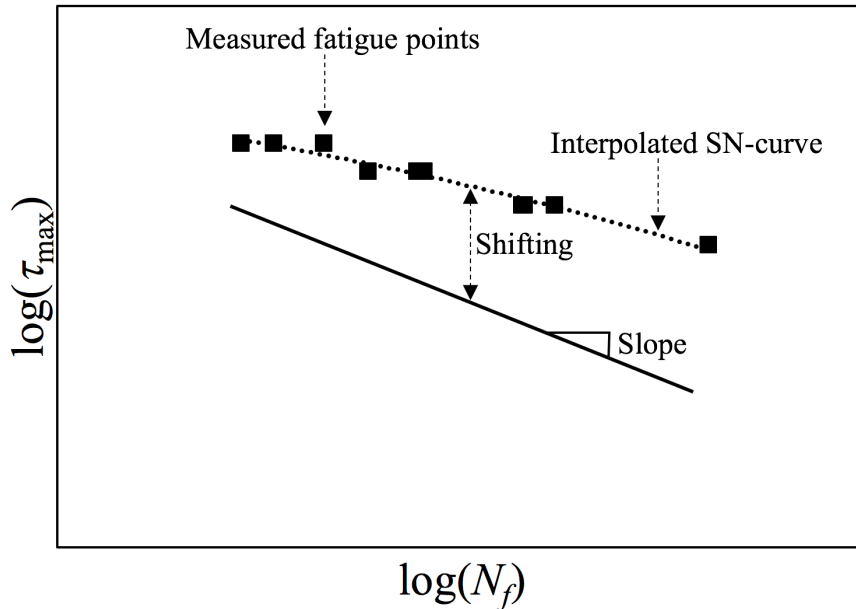


Figure 2.4: Schematic of fatigue curves.

### 2.3.6 This work's contribution to a multiscale model

This thesis is part of a bigger project that aims to develop a new approach based on a multiscale analysis to predict long-term behavior of composites. The contribution of this thesis is to increase the understanding of how water and heat affect the static and fatigue behavior of composites, thus potentially discover new aspects that must be considered and included in the multiscale model. In addition, the data obtained in this work can be used to evaluate the validity of the model.



## 3 Experimental

### 3.1 Material

In this work, a glass fiber/epoxy laminate was used for all the experiments. This particular composite was chosen as it is typically used for marine applications [23]. The epoxy resin system consisted of EPIKOTE resin MGS RIMR 135 mixed with EPIKURE curing agent MGS RIMH137. E-glass (3B HiPer-tex<sup>TM</sup>) unidirectional fiberglass fabric was used as the fiber. The constituent properties can be seen in table 3.1. The properties were mainly found in the resin's and fiber's datasheet. If values were not found in the datasheets, estimated values were taken from the literature from similar materials. The reference for each material property is specified in the table.

Table 3.1: Constituent properties of the glass/epoxy laminate used in this work.

	<b>E</b> [GPa]	$\nu_{12}$	<b>G<sub>12</sub></b> [GPa]	$\sigma_U$ [MPa]	$\sigma_Y$ [MPa]	$\rho$ [g/cm <sup>3</sup> ]
<b>Fiber</b>	90 [33]	0.2 [4]	37.5	2800 [33]	-	2.58 [33]
<b>Matrix</b>	2.8 [34]	0.35 [4]	1.1	60 [34]	35 [35]	1.20 [34]

### 3.2 Preparation of the composite laminate

The composite laminate used in this work was manufactured by vacuum infusion as described in the following. First, a flat steel plate (the mold) was cleaned with acetone in order to remove unwanted dirt or residue that could compromise the quality of the laminate. Then, a thin layer of release agent (RenLease QV 5110) was spread out in the mold in order to ease the demoulding process. 32 plies of fiberglass fabric were cut and laid up. Each layer had a 0° orientation. A flow mesh was laid on top of the fiberglass fabric pile to ensure a steady flow of resin. A peel ply was laid between the last layer of fiber fabric and the flow mesh. Again, this was done to ease the demoulding process. Sealant tape was attached to the mold, surrounding the stack of plies. A vacuum bagging film was then placed on top of the stack, attached to the tape and ensuring an airtight system. Figure 3.1 shows a scheme of the system. An inlet and an outlet pipe were attached to the system. At the inlet and outlet, T-junction connectors attached to spiral wraps were utilized to ensure resin flow over the entire width of the laminate. A piece of fiberglass fabric was placed between the inlet/outlet piping and the bagging film to prevent sharp edges of the piping to induce leaks in the bagging film.

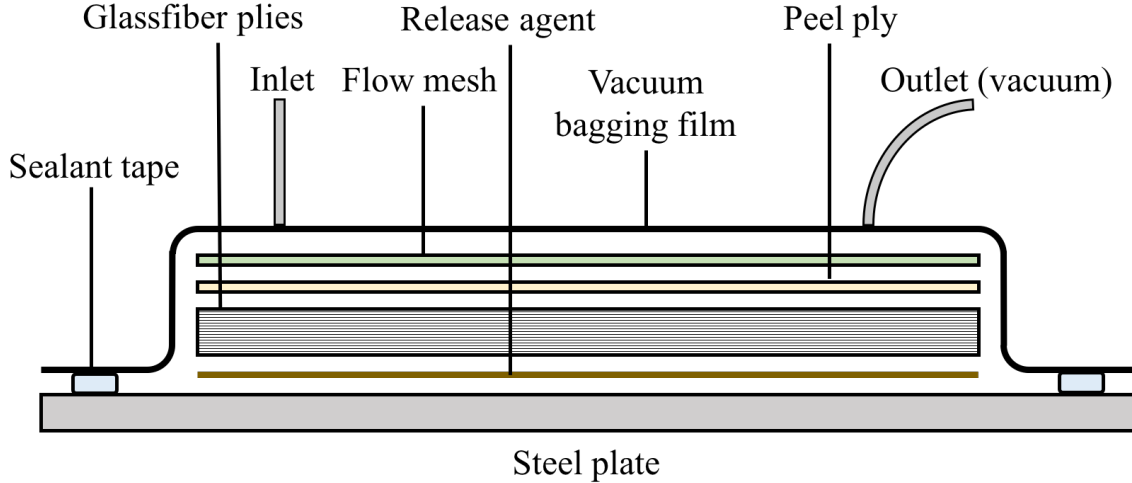


Figure 3.1: The vacuum bagging system set-up used in this work.

When the pile shown in figure 3.1 was completely laid up, vacuum was applied to the system by a vacuum pump. After checking that no leak was present, the resin and curing agent were mixed in a 100:30 weight ratio. The epoxy resin system was stirred for five minutes and subsequently degassed for 30 minutes at  $-0.95$  atm. The pressure gradient followed the fiber direction to ensure a decent infusion rate. The inlet pipe was then immersed in the uncured epoxy, and the resin infusion process was subsequently started. When the infusion process was complete, the composite laminate was cured at room temperature for 24 hours. After that, the laminate was demoulded and finally cured in a ventilated oven at  $80^{\circ}\text{C}$  for 16 hours according to the resin’s technical datasheet [34].

### 3.3 Preparation of I-beam specimens

In this work, I-beam specimens were tested in a four-point bending configuration to find the material’s interlaminar shear behavior. Usually, short beams shear tests are performed with specimens having a rectangular cross section according to ASTM D2344 [9]. As mentioned in section 2.2, the time to reach saturation is highly dependent on the thickness in the diffusion direction. Preparing specimens with the minimum thickness allowed by ASTM D2344 results in specimens highly vulnerable to destructive roller indentation. To avoid this effect, without increasing the conditioning time, I-beam specimens were proposed and utilized in this work. How these specimens were prepared from the laminate is described in the following. Note that due to limitations in time, the specimens were made from two different laminates. From now on these laminates are referred to as laminate A and laminate B. Laminate A is produced by Gagani, while laminate B is produced by the author with the same constituents and method as laminate A.



A diamond saw cutting machine was used to cut the laminate into 300 mm long beams with a width of approximately 20 mm. Then, the beams were milled down to a rectangular cross-sectional area equal 15 mm  $\times$  20 mm with an end milling tool. Note that the plies were perpendicular to the direction of the height, see figure 3.3. A smaller end milling tool was used to cut the grooves with the dimensions as seen in figure 3.2. The cuts had an axial depth of 0.5 mm and a feed rate of 160 mm/min until the last cut of each surface, which had a 0.2 mm axial depth and a 80 mm/min feed rate. This was done to reduce the creation of microcracks that can, potentially, act as stress concentrations. The beams were cut with a cutting machine into short I-beams with a length of approximately 63 mm. Finally, the ends of the beams were ground and polished to remove microcracks caused by the cutting. Grinding paper of increasing fineness (P500, P1000, P2000, P4000) was used for the grinding, and water was used as the lubricant. For the polishing, 3  $\mu$ m polishing disks with diamond paste suspensions were used, with a DP-Lubricant Blue as a lubricant. The grinding and polishing resulted in beams with the length of 60 mm.

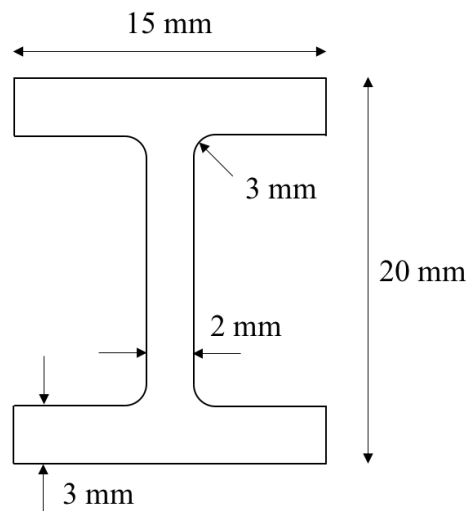


Figure 3.2: I-beam dimensions, the length of the beams were 60 mm.

### 3.4 Sample conditioning

28 I-beam specimens from laminate A were conditioned in a water bath, and will be referred to as wet samples from now on. Prior to conditioning, these specimens were dried in an oven at 50°C for 72 hours. This was done to remove some of the initial moisture in the specimens induced by the laboratory atmosphere and the water cooling from the machining process. At the end of the drying interval, the specimens were removed from the oven and immediately weighed. Each measurement was recorded. After that, the specimens were submerged in the liquid bath. Distilled water was used as the liquid in this

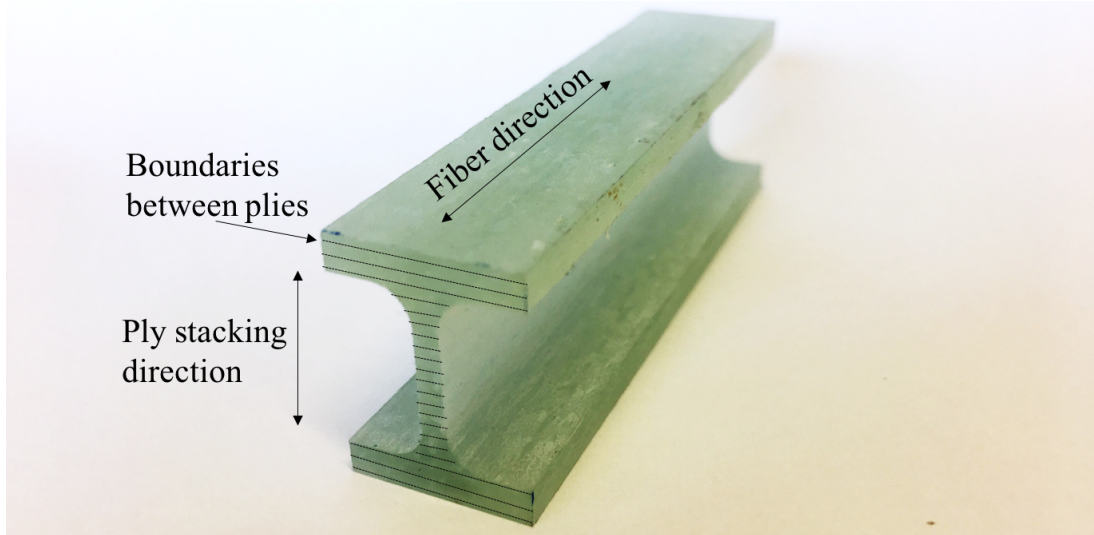


Figure 3.3: I-beam fiber and ply stacking direction.

work. The temperature in the conditioning chamber was kept constant at  $60^{\circ}\text{C}$  by the help of an electrical resistance and a PID controller. Hence, the conditioning temperature was  $25^{\circ}\text{C}$  below the material's glass transition temperature, which is recommended practice in ASTM D5299 [36]. The specimens were occasionally taken out of the bath, wiped free of surface moisture with an absorbent towel, and immediately weighed in order to monitor the water uptake. The scale used in this work was a Mettler Toledo AG204 DeltaRange with an accuracy of  $1/10000$  g. After three months of conditioning, the samples were taken out of the bath and tested as described in section 3.6.

### 3.5 Volume fraction measurement

The volume fraction of the laminates was measured by performing a burn-off test according to ASTM D3171 [37]. This implies that a material sample from each laminate was subjected to  $550^{\circ}\text{C}$  for 5 hours. As a result, the epoxy fully evaporated, and it was possible to calculate the volume fraction by weighing the samples before and after the test. Laminate A had a fiber volume fraction of 0.59, whereas laminate B had a fiber volume fraction of 0.54. The variation in volume fraction is not ideal, but assumed to be within an acceptable range. The properties of interest in this work, i.e. shear properties, are matrix dominated and therefore not very influenced by the fiber volume fraction [3]. Furthermore, samples from both laminate A and B were tested and compared, and the results are reported in section 4.3.2.

## 3.6 Four-point bending

### 3.6.1 General setup

In order to test the interlaminar shear strength of the beam, a four-point bending fixture similar to the one described in ASTM C393 was utilized [38]. 10 mm rollers were used for both support and load. Upper and lower span distances are shown in figure 3.4. An anti-buckling device was used during testing to prevent the web from buckling out from its position and is shown in figure 3.5. The anti-buckling device allowed the beam to undergo a deflection of about 3 mm until the walls of the device touched the top flange of the specimen. A deflection of 3 mm was confirmed to be larger than the deflection at failure for every test environment, see section 4.3.1.

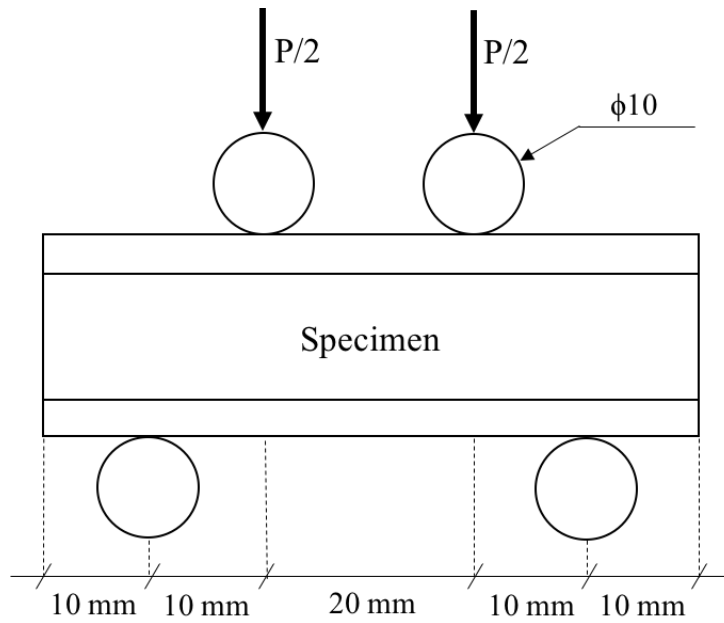


Figure 3.4: Schematic showing the distances between rollers.

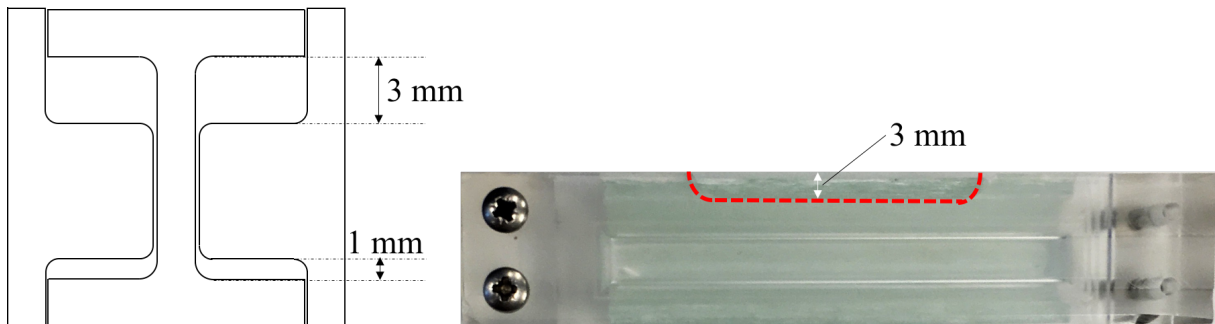


Figure 3.5: Anti-buckling device.

Four-point bending of the dry and wet specimens was conducted in two separate setups. The dry tests were performed in an MTS servohydraulic system (50 kN load cell)

combined with an MTS environmental chamber which enabled temperature control with a tolerance of  $\pm 1^\circ\text{C}$ , see figure 3.6. For the wet tests, a waterproof chamber enclosing the bending fixture was built and inserted into a Shenck 12.5 kN load cell, see figure 3.7. An inlet and outlet of the chamber were connected to a temperature controlled (tolerance  $\pm 1^\circ\text{C}$ ) bath and an aquarium pump, ensuring a continuous flow of water at a desired temperature around the four-point bending fixture. Prior to testing, specimens were installed in the test set-up for 10 – 15 minutes to allow the material to reach the desired test temperature. The axial displacement and applied load were measured and recorded by the test machine's built-in sensors.

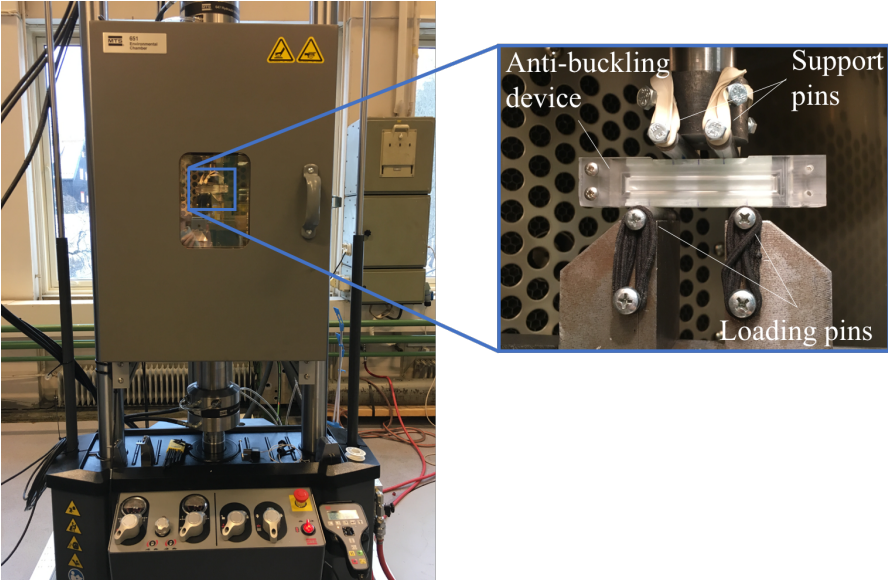


Figure 3.6: Test set-up for dry testing.

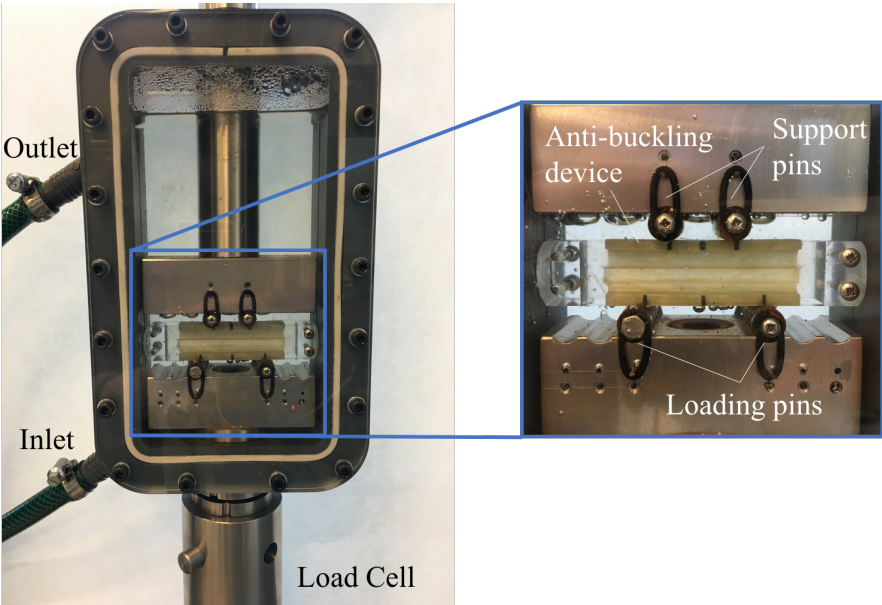


Figure 3.7: Test set-up for wet testing.

When a beam is subjected to a four-point bending, the transverse loads cause resultant shear forces and moments in the beam as illustrated by the diagrams in figure 3.8. The shear forces cause a shear stress distribution over the cross-section as seen in figure 3.9. The shear stress can be calculated by Zhuravskii's shear stress equation as in ASTM 2344 [9, 39]. The equation is given as

$$\tau = \frac{VS}{It} \tag{3.1}$$

where  $V$  is the shear force,  $S$  is first moment of area,  $t$  is thickness and  $I$  is the second moment of inertia of the cross-section. The maximum shear stress is experienced when  $V = P/2$ ,  $t$  is the thickness of the web and  $S$  is calculated in relation to the neutral axis of the cross section. The maximum shear stress in the beam can consequently be calculated by equation 3.1 as

$$\tau = 0.015351P \tag{3.2}$$

with the fillets being ignored.  $P$  is the load applied by the test machine.

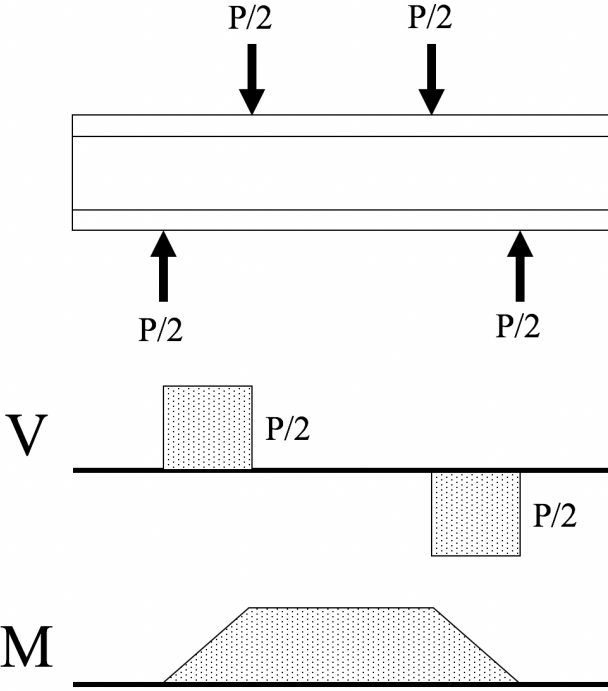


Figure 3.8: Shear force and bending moment diagram of the I-beam.

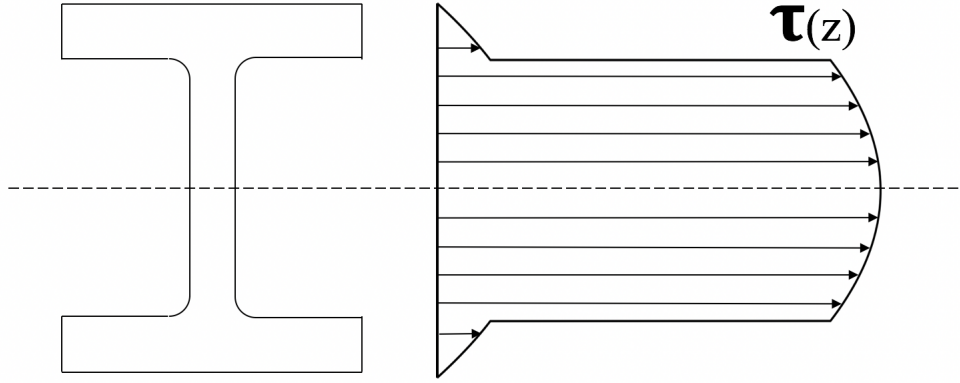


Figure 3.9: Shape of shear stress distribution over the beam's cross-section.

The shear modulus was calculated by Timoshenko beam theory, where the deflection of the beam is said to be the sum of deflection caused by bending and deflection caused by shear. It can be calculated by the following formula

$$\delta = \delta(M) + \delta(V) = \int_L \frac{M}{EI} dx + \int_L \frac{V}{GA} dx \quad (3.3)$$

where  $\delta$  is the deflection of the beam (measured as displacement of the test machine),  $M$  is the bending moment caused by the transverse forces,  $E$  is the tensile modulus,  $L$  is the length of the beam,  $V$  is the resultant shear force,  $G$  is the shear modulus and  $A$  is the area of the cross-section. By assuming that the deflection caused by bending is zero, it is possible to calculate the shear modulus as

$$G = \left( \frac{\Delta P}{\Delta \delta} \right) \frac{L}{2A} \quad (3.4)$$

where  $\frac{\Delta P}{\Delta \delta}$  is the slope of the load-deflection curve measured during the four-point bending test. The assumption that the deflection caused by bending is zero is somewhat questionable, considering that the distribution between the shear's and the bending's contribution to deflection is unknown. However, this assumption will be more appropriate for shorter beams, where shear deformation is more prominent than in longer beams. In addition, this is the only analytical method to obtain shear modulus in a four-point bending known to the author. It is therefore utilized in this work while being aware of its limitations.

### 3.6.2 Static testing

Some of the prepared specimens were tested statically. An overview of the number of tested specimens in each test environment is seen in table 3.2. Whether the specimens were made from laminate A or B is indicated in the parentheses in the table. Note that four specimens were conditioned for a full year before they were tested in order to examine the effect of water ingress beyond saturation. These specimens were prepared and conditioned by Gagani prior to the start-up of this work.

The static tests were executed by utilizing displacement control at a speed of 1 mm/min. The specimens were bent until a severe reduction in strength was observed.

Table 3.2: Overview of the number of static tests performed in this work and what laminate is used for the different tests.

	<b>RT</b>	<b>40 deg</b>	<b>60 deg</b>
<b>Dry</b>	4 (B)	4 (B)	4 (B)
<b>Wet</b>	-	4 (A)	4 (A)
<b>Wet - 1 year</b>	4 (A)	-	-

### 3.6.3 Fatigue testing

For the fatigue testing, the specimens were subjected to a sinusoidal cyclic load control. The cyclic load had a stress ratio of  $R = 0.1$  and a frequency of 4 Hz. For composites, it is important to keep the loading frequency low to avoid internal heat generation in the specimen [40]. When a test reached 2 million cycles without the sample failing, it was stopped and considered a runout. The specimens were bent until reaching a deflection of 3 mm, which is the limit of the anti-buckling device. A complete separation of the samples, as often seen in tensile testing, will never occur in a four-point bending shear test. A deflection limit believed to ensure that the material failed was therefore chosen.

An overview of the number of tested specimens in each test environment is seen in table 3.3. Whether the specimens were made from laminate A or B is indicated in the parentheses in the table.

Table 3.3: Overview of the number of fatigue tests performed in this work and what laminate is used for the different tests..

	<b>40 deg</b>	<b>60 deg</b>
<b>Dry</b>	10 (B)	8 (B)
<b>Wet</b>	11 (A)	7 (A)

### 3.7 Damage analysis

One fatigue test specimen from each test environment was examined in a confocal microscope (Alicona InfiniteFocus G4) after failure in order to study the failure mode. The inspected specimens were cut with a circular water-cooled diamond saw 15 mm from the beam's end, as seen in figure 3.10. The reason for choosing this location is that the maximum shear force occurs at that location (see figure 3.8). After cutting, the specimens were embedded in a polymer resin, cured and subsequently ground and polished (with the same procedure as described in section 3.3). The surfaces were inspected using a magnification of 5x. In addition, the specimens were inspected by placing them on top of a light-table. If the material was damaged, e.g. cracked or delaminated, the backlight would scatter and appear as dark spots in the composite [41].

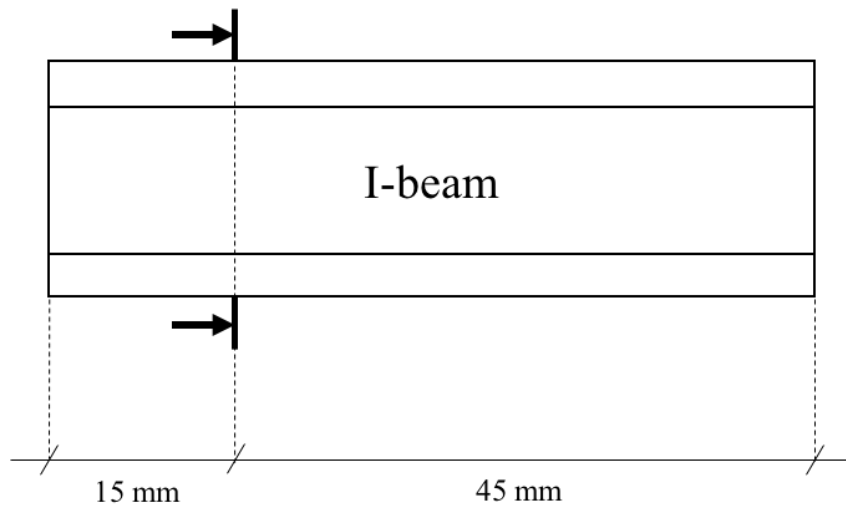


Figure 3.10: Schematic showing the representative cross-section for micrographs.



## 4 Results

### 4.1 Introductory remarks

In this chapter, the experimental results obtained in this study will be presented. Where beneficial, data obtained by Abedin Gagani will be presented alongside the data obtained by the author of this thesis. Gagani's results include the following:

- Static results for wet specimens at room temperature
- Fatigue results at room temperature, both wet and dry

All other results are obtained by the author unless otherwise noted.

### 4.2 Water uptake

#### 4.2.1 Analytical model

An analytical model for the water uptake in the I-beam was created and is presented in the following. In order to utilize equation 2.16 and 2.17 for the beam's geometry, it was divided into rectangular sections as seen in figure 4.1. It was assumed that the water uptake in the web and the flanges were independent of each other, and their separate water uptake was added together to give the total water uptake of the beam. The web was modeled as a rectangular parallelepiped having diffusion from four of the six sides, hence suiting the 2D equation 2.16. The flanges were modeled as fully submerged rectangular parallelepipeds, hence suiting the 3D equation 2.16. The fillets were ignored in this model.

A two and three dimensional solution to Fick's equation is given by Blikstad et al. [22]. Adding these solutions together yields

$$M(t) = \frac{2M_{fl}(t)t_{fl}w_{fl} + M_w(t)t_w h_w}{2t_{fl}w_{fl} + t_w h_w} \quad (4.1)$$

where,

$$M_{fl}(t) = M_{eq} \left[ 1 - \left( \frac{8}{\pi^2} \right)^3 \sum_{i=0}^{\infty} \sum_{j=0}^{\infty} \sum_{k=0}^{\infty} C_i^{fl} D_j^{fl} E_k^{fl} \right] \quad (4.2)$$

$$M_w(t) = M_{eq} \left[ 1 - \left( \frac{8}{\pi^2} \right)^2 \sum_{i=0}^{\infty} \sum_{j=0}^{\infty} C_i^w D_j^w \right] \quad (4.3)$$

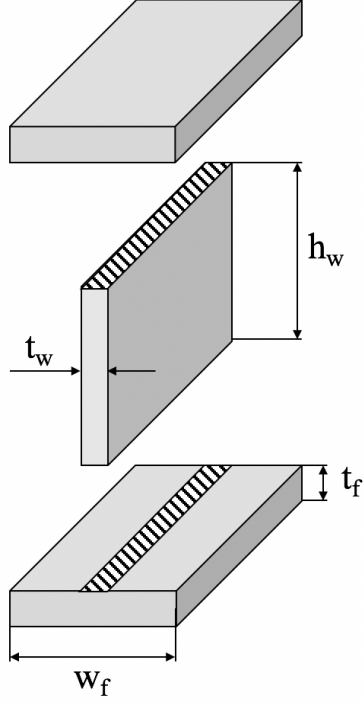


Figure 4.1: Schematic showing the sections for the analytical water uptake solution.

where,

$$C_i^{fl} = \frac{\exp[-(2i+1)^2(\frac{\pi}{L})^2 D_{11}t]}{(2i+1)^2} \quad (4.4)$$

$$D_j^{fl} = \frac{\exp[-(2j+1)^2(\frac{\pi}{w_{fl}}) D_{22}t]}{(2j+1)^2} \quad (4.5)$$

$$E_k^{fl} = \frac{\exp[-(2k+1)^2(\frac{\pi}{t_{fl}}) D_{33}t]}{(2k+1)^2} \quad (4.6)$$

$$C_i^w = \frac{\exp[-(2i+1)^2(\frac{\pi}{L}) D_{11}t]}{(2i+1)^2} \quad (4.7)$$

$$D_j^w = \frac{\exp[-(2j+1)^2(\frac{\pi}{t_w}) D_{22}t]}{(2j+1)^2} \quad (4.8)$$

where  $D_{11}$ ,  $D_{22}$  and  $D_{33}$  are the components of the diffusivity matrix and  $M_{eq}$  is the moisture saturation content of the composite. These constants were found in research performed by Gagani et al., where diffusion analysis of the same material in the same conditioning environment as in this work (distilled water at 60°C) was performed [23].  $D_{11}$ , the diffusivity in the fiber direction, was found to be 0.002 mm<sup>2</sup>/h.  $D_{22}$  and  $D_{33}$  are the diffusivities in the direction perpendicular to the fibers and were found to be = 0.0045 mm<sup>2</sup>/h.  $M_{eq}$  was calculated from the equation [42]

$$M_{eq} = M_{eq}^M \frac{(1 - V_f)\rho_m}{V_f\rho_f + (1 - V_f)\rho_m} \quad (4.9)$$

where  $M_{eq}^M$  is the matrix diffusion constant equal 3.18%. With  $V_f = 0.59$ ,  $\rho_m = 1.2 \text{ g/cm}^3$  and  $\rho_m = 2.58 \text{ g/cm}^3$ , equation 4.9 gave a moisture saturation content of 0.777%. All of the above-mentioned constants were obtained by fitting experimentally obtained weight gain curves, obtained from plates having different material orientations, to the solution of the Fickian diffusion equation. With these material constants, equation 4.1 gave an analytical solution to the water uptake in the composite. The solution is plotted in figure 4.2. According to this solution, saturation in the I-beams should be reached after  $\approx 30 \text{ h}^{1/2} = 37.5$  days of conditioning.

#### 4.2.2 Experimental

The specimens were weighed during conditioning. The moisture content at a given time,  $M(t)$ , was calculated by

$$M(t) = \frac{W(t) - W_0}{W_0} \quad (4.10)$$

where  $W(t)$  is the mass of the specimen at a given time and  $W_0$  is the oven dry specimen mass. The results are shown in figure 4.2. The blue dots show the mean weight gain, and the error bars show the standard deviation of the measurements. As seen from the graph, the specimens did not seem to saturate as the experimental weight gain curve never stopped increasing. However, the specimens were taken out of the conditioning chamber after approximately three months and subsequently tested. The validity of this is discussed in 5.1.

Testing of the wet specimens was carried out over a total of 25 days. As a consequence, the last tested specimens had an additional conditioning time at the time of testing. The four last specimens were weighed shortly before testing, and the results are seen in figure 4.2 as gray crosses. Their estimated weight gain curves during these 25 days are illustrated as the grey dashed lines. The mass increased during this period, as expected.

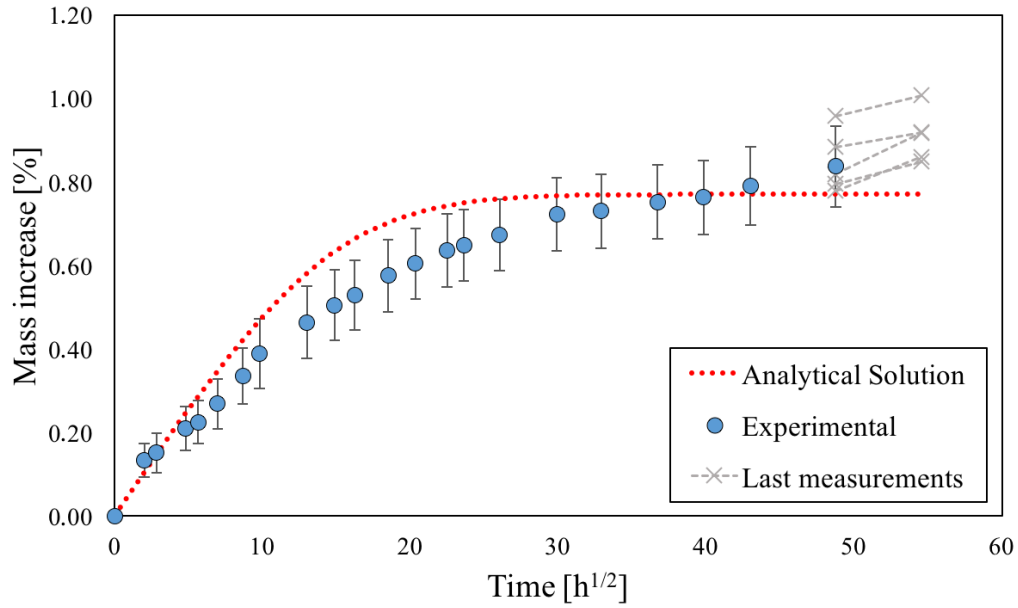


Figure 4.2: Experimental and analytical water uptake as mass increase versus time of immersion.

After three months in the water bath, the specimens showed a discoloration, see figure 4.3. Discoloration is a result of the degradation and is attributed to a hygrothermal effect called thermal oxidation [43]. The discoloration has shown to be irreversible for the material tested in this work, but the mechanisms leading to the color change has shown to not affect its mechanical behavior [44]. However, the possibility that these mechanisms affect the material in the very long term can not be excluded.

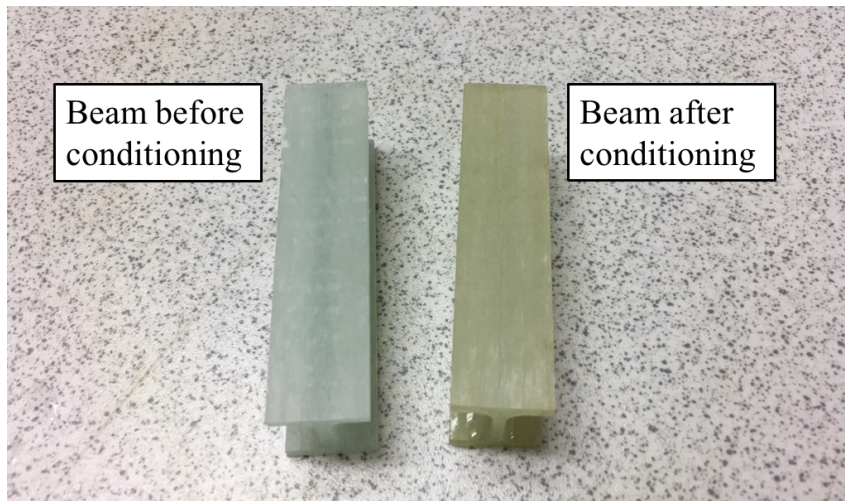


Figure 4.3: The I-beam before and after conditioning.

### 4.3 Static behavior

#### 4.3.1 Main results

Static tests were performed as described in section 3.6. All the measured shear stress-deflection curves for each test environment are given in figure 4.4. It is seen that the specimens exhibited a non-linear shear response, which is common for composites [45].

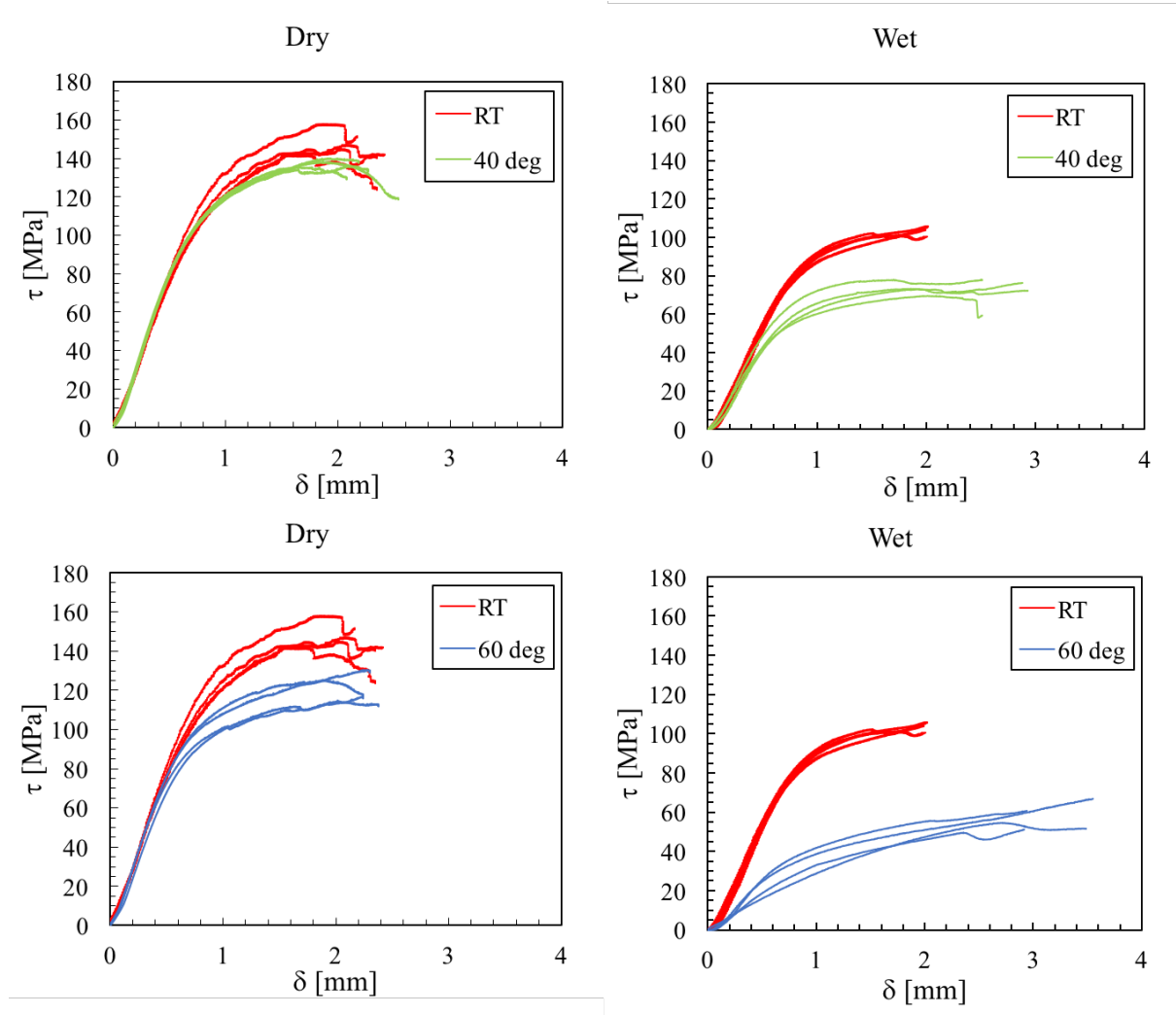


Figure 4.4: Shear stress-deflection curves for different environments.

Based on the stress-deflection curves, the mean ultimate shear strength for each environment was found. They are reported as bar charts in figure 4.5. Values for each tested specimen are found in table 8.1 in the Appendix. The beam's shear strength, denoted  $\tau_{max}$ , was defined as the sample's maximum obtained shear stress. If no clear maximum was observed,  $\tau_{max}$  was defined as the value where the stress-deflection curve first read a negative slope. The shear strength's corresponding deflection, from now on referred to as deflection at failure and denoted  $\delta_f$ , is reported in figure 4.6. For the dry samples,

an increase in test temperature from RT to 40°C and 60°C resulted in a reduction in  $\tau_{max}$  of 9% and 24%, respectively. Increasing the test temperature from RT to 40°C and 60°C resulted in a 28% and 48% drop in  $\tau_{max}$  for the wet samples, respectively. The wet samples were more affected by the temperature increase compared to the dry samples. By comparing the dry and the wet samples, it was observed that conditioning led to a reduction in  $\tau_{max}$ . This effect was more severe for higher testing temperatures. The deflection at failure,  $\delta_f$ , increased by an increase in test temperature. Conditioning also resulted in an increase in  $\delta_f$  for all test temperatures except RT.

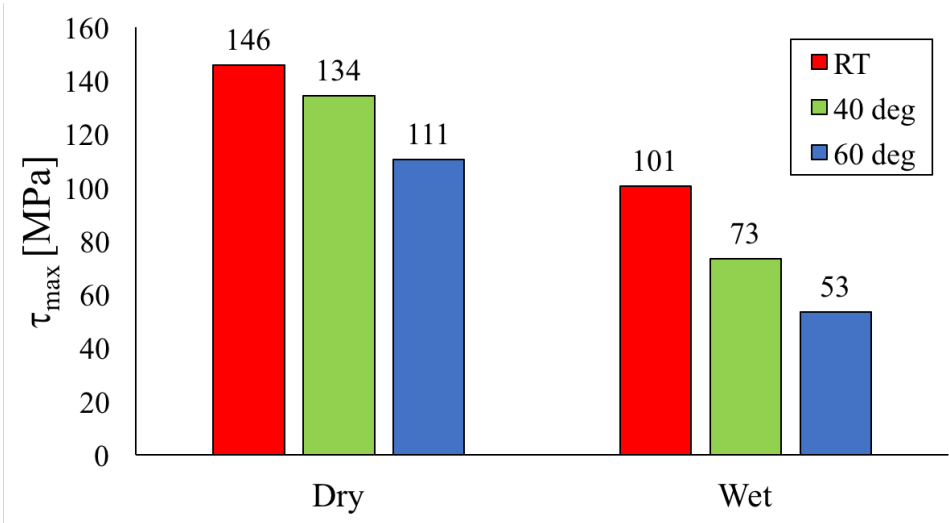


Figure 4.5: Mean shear strength for different environments.

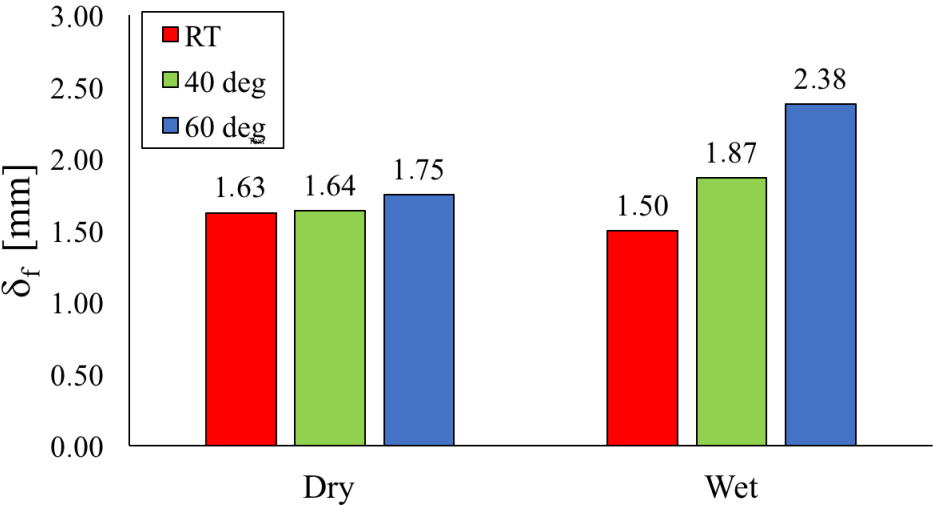


Figure 4.6: Mean deflection at failure for different environments.

The yield strength,  $\tau_Y$ , for each performed test was obtained by visual inspection of the stress-deflection curve.  $\tau_Y$  was defined as the load level where the load-deflection curve changed from being linear to non-linear. The  $\tau_Y$  values for the different test environments are presented as bar charts in figure 4.7. For the dry samples,  $\tau_Y$  decreased by 1% and 12% by increasing the test temperature from RT to 40°C and 60°C, respectively. For the wet samples,  $\tau_Y$  decreased by 38% and 67% for the samples tested at 40°C and 60°C, respectively. Hence, the yield strength of the wet samples was more influenced by the change in test temperature compared to the dry samples'. By comparing the dry and wet samples, it was evident that conditioning resulted in a reduction in  $\tau_Y$ . This effect was more severe for higher test temperatures.

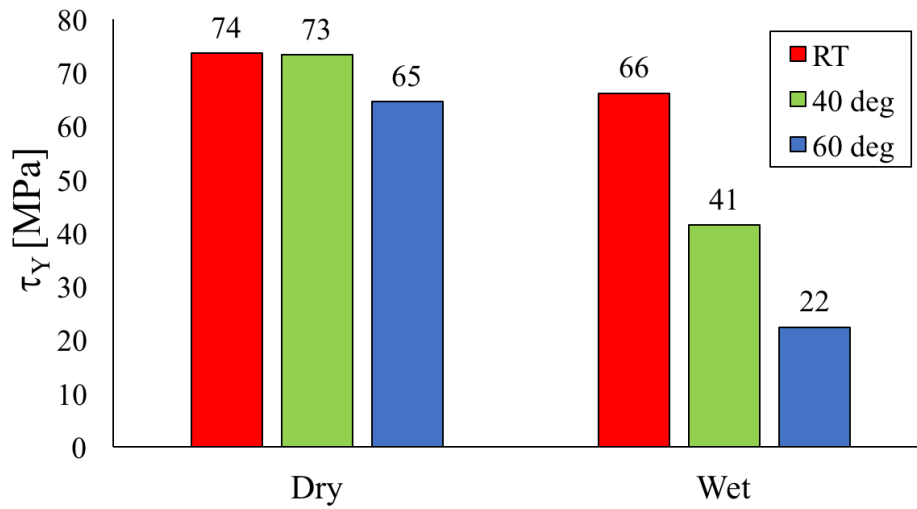


Figure 4.7: Mean yield strength for different environments.

The shear modulus,  $G_{12}$ , was calculated for each test environment. The values are found in figure 4.8.  $G_{12}$  was calculated by equation 3.4, where  $\frac{\delta P}{\Delta \delta}$  is the tangent of the linear part of the stress-deflection curve. For the dry samples,  $G_{12}$  was not significantly affected by an increase in temperature. Note that the dry samples tested at 40°C seemed to be 1% stiffer than the samples tested at RT, while the samples tested at 60°C were 6% less stiff than the ones tested at RT. A 1% increase or decrease in  $G_{12}$  is seen as an insignificant change. The stiffness of the wet samples was more influenced by the temperature increase than the stiffness of the dry samples. For the wet samples, an increase in test temperature from RT to 40°C and 60°C resulted in a reduction in  $G_{12}$  of 14% and 58%, respectively. By comparing the stiffness of the dry and the wet samples, it was evident that conditioning resulted in a reduction in  $G_{12}$ . This effect was more severe for higher test temperatures.

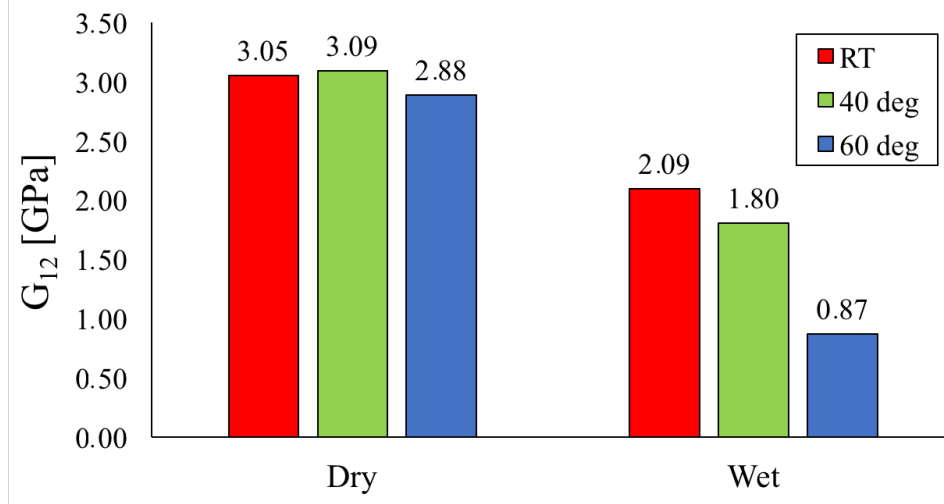


Figure 4.8: Mean shear modulus for different environments.

$\tau_{max}$  and  $G_{12}$  were calculated by Chamis' theory (equation 2.2-2.3) and Huang's theory (equation 2.4-2.10) and are reported in table 4.1. Note that the values were calculated from the constituent material properties found in table 3.1 for a composite having a fiber volume fraction equal 0.54. The input value  $\tau_{max}^m$  was not found for the epoxy studied in this work, and was therefore estimated to be 50 MPa based on values for similar materials found in the literature [46].  $E_T^m$  was assumed to be 1/3 of  $E_m$ . All of the constituent properties in table 4.1 are given for room temperature, thus the calculated values are representative for room temperature.

It is seen that the experimentally obtained  $\tau_{max}$  is three to four times greater than the ones obtained by the micromechanical models. Note that the experimentally obtained  $\tau_Y$  for dry samples at room temperature is much closer to the values for  $\tau_{max}$  obtained by the micromechanical models. Regarding  $G_{12}$ , the experimentally and analytically obtained values seem to coincide better. These results will be further discussed in section 5.3.

Table 4.1: Experimentally and analytically obtained shear strength and modulus at room temperature.

	$\tau_{max}$ [MPa]	$G_{12}$ [GPa]
<b>Chamis</b>	41	3.84
<b>Huang</b>	43	3.38
<b>Experimental</b>	146	3.05



### 4.3.2 Comparison of laminate A and B

Static tests at RT of samples made from both laminate A and B were conducted, and their stress-deflection curves are plotted together in figure 4.9. The results of laminate A is obtained by Gagani. It is seen that the stress-deflection curves followed each other until reaching a deflection equal  $\delta_f$ , where the curves of laminate A seemed to increase while the curves of laminate B decreased. The reason for this divergence is the anti-buckling device used during testing. The anti-buckling device used during testing of laminate A did not allow the beam to deflect as much as the anti-buckling device used during testing of laminate B, hence the last part of laminate A's curves are influenced by the anti-buckling device. The  $\tau_{max}$  of laminate A and B were very consistent, namely 146 MPa and 147 MPa. The values of  $G_{12}$ ,  $\tau_Y$  and  $\delta_f$  were not as consistent. All of the above-mentioned values are found in table 4.2.

Table 4.2: Static properties of laminate A and B.

	Laminate A	Laminate B
$\tau_{max}$ [MPa]	147	146
$G_{12}$ [GPa]	2.41	3.05
$\delta_f$ [mm]	1.225	1.625
$\tau_Y$ [GPa]	105	74

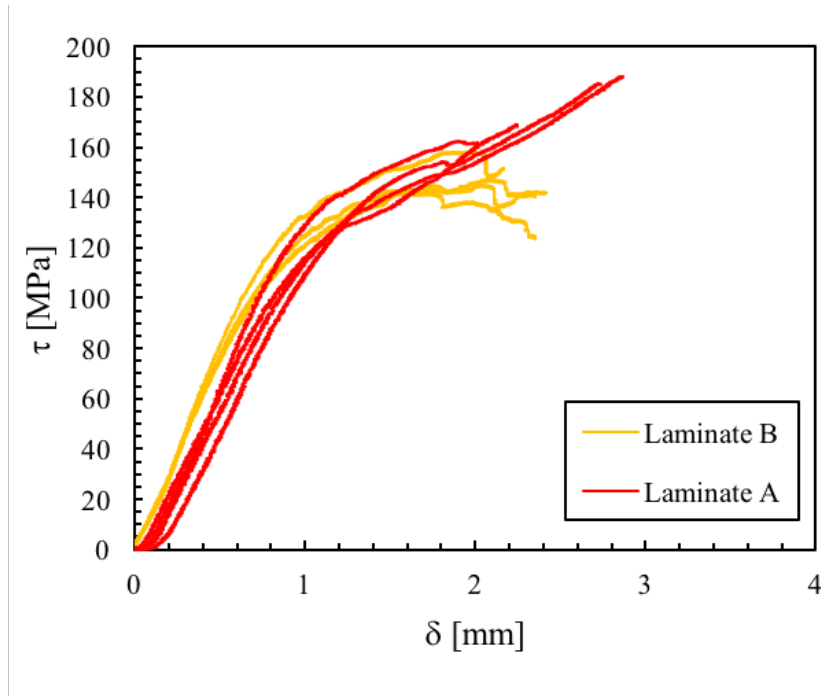


Figure 4.9: Stress-deflection curves of samples made from laminate A and B.

### 4.3.3 Static tests of beams immersed in water for one year

Four beams conditioned for almost a full year ( $\approx 92 \text{ h}^{1/2}$ ) were tested statically. After three months of conditioning, the beams had an average mass percentage of water of 0.73. After a full year of conditioning, the beams had an average mass percentage of water of 1.33. This is a dramatic weight gain that clearly demonstrates that the beams did not saturate after three months of conditioning. The results of the static shear tests are presented in figure 4.10, together with the stress-deflection curves of the beams tested after three months of conditioning. The stress-deflection curves for samples conditioned for one year did not have a clear maximum, nor a clear negative slope. However, it is seen that the curve flattens out at approximately 60 MPa before it starts increasing again. With this plateau defined as  $\tau_{max}$  of the samples, it resulted in a 40% decrease in strength compared to the samples conditioned for three months. This is a dramatic drop in strength. It is seen that the values of  $G_{12}$  and  $\tau_Y$  decreased as well.

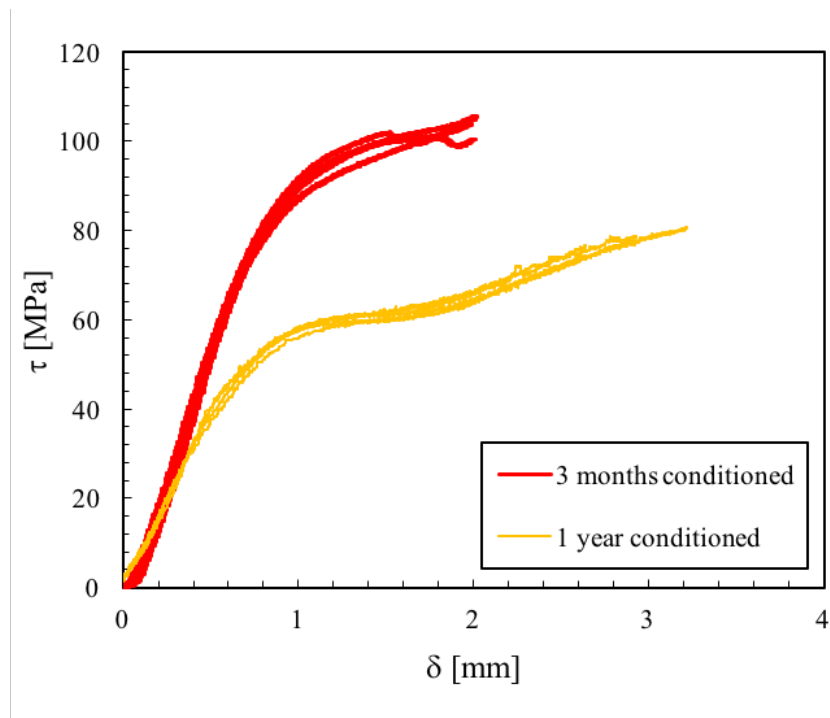


Figure 4.10: Stress-deflection curves of samples conditioned for three months and one year.

## 4.4 Fatigue behaviour

### 4.4.1 Introductory remarks

As mentioned earlier, every specimen was bent until a deflection of 3 mm was reached in the fatigue bending tests. It was done to ensure that the specimens actually failed, and to avoid stopping the fatigue tests prematurely. However, in the following analysis of the fatigue results, the author chose to subtract and report the fatigue data obtained until a deflection equal the statically obtained  $\delta_f$  (reported in figure 4.6) was reached. This applies for every fatigue data discussed in the following subsections. The choice of failure limit is elaborated and further discussed in section 5.2.

### 4.4.2 Fatigue life

The results of the fatigue tests performed in this study are presented in a  $\log(\tau_{max})$ - $\log(N_f)$  plot in figure 4.11. Runouts (samples reaching two million cycles) are labelled with arrows. Note that some specimens were tested with a slightly different R-ratio due to errors in the load cell. These values are specified in table 8.2-8.3 in the Appendix along with the fatigue data for each specimen. The fatigue data were interpolated to equation 2.18 with  $\tau$  as the independent variable. Note that runouts were not included in the regression. Details from the regression are given in table 4.3 and the interpolated curves are plotted together with the fatigue data in figure 4.11.

For the SN-curves of the dry specimens, an increase in test temperature shifted the curve downwards. Increasing the test temperature from RT to 40°C, lead to a 40 times shorter lifetime for the same applied stress. Increasing the test temperature from 40°C to 60°C, lead to a 200 times shorter lifetime for the same applied stress. For a given number of cycles, the samples tested at 40°C failed at 80–90 % of the applied stress that the samples failed at in RT. The samples tested at 60°C failed at 70% of the applied stress that the samples tested at 40°C failed at, for a given number of cycles. A similar downward shift due to an increase in test temperature applied to the SN-curves for the wet specimens. However, the downward shift was more dramatic for the curves representing the wet samples. By comparing the SN-curves of the dry and wet samples, it is seen that the SN-curve experienced a downward shift as a consequence of the conditioning.

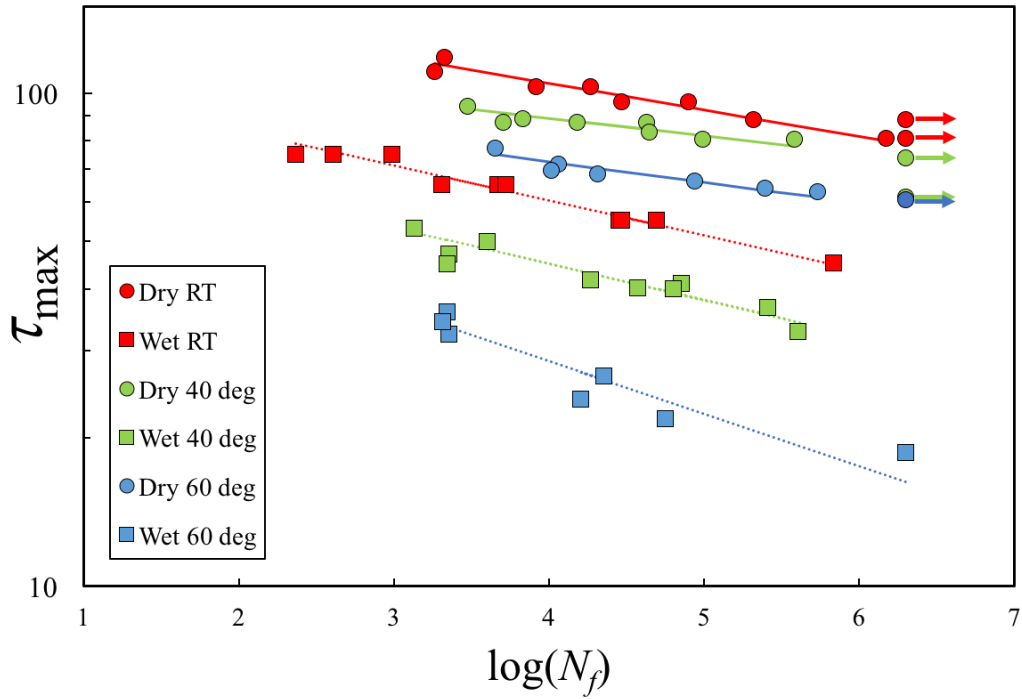


Figure 4.11: Fatigue data and SN-curves for different environments.

Table 4.3: Model parameters and R-squared values from the linear regression of each SN-curve.

Test environment	$\tau_0$ [MPa]	1/k	$R^2$
Dry RT	171.7	0.05383	0.9506
Wet RT	116.5	0.07114	0.9403
Dry 40 deg	123.0	0.03546	0.8011
Wet 40 deg	88.5	0.07337	0.8543
Dry 60 deg	106.8	0.04198	0.8811
Wet 60 deg	76.1	0.10648	0.8852

### 4.4.3 Damage analysis

In figure 4.12, a light transmittance photo of one specimen at each test environment is presented. All of the depicted specimens endured an intermediate number of cycles, that is 20,000 – 60,000 cycles. This equaled a stress level in the area 62% to 65% of the ultimate strength ( $\tau_{max}$ ) for the dry samples, and a stress level in the area 50% to 55% of the ultimate strength for the wet samples. The represented specimens' light transmittance was typical for their respective test environment, and the light transmittance of all other specimens tested in this work can be seen in figure 8.1 in the Appendix. The samples tested at RT were not bent until a deflection of 3 mm was reached, as was the case with the other samples, and should be taken into consideration. As mentioned earlier, the observed dark areas indicate damage in the composite material. The damage-area was mainly located in the central web between the rollers, where maximum shear force occurred, as seen in figure 3.8. It is seen that the damage-area increased with an increase in test temperature for the dry specimens, while it is uncertain if this was the case for the wet specimens. The distribution of damage was less regular for the dry specimens compared to the wet ones. In addition, the damage-area of the dry samples was distributed all the way to the beams' end, which was not the case for the wet beams. A clear crack was visible at the dry beams' ends, as seen in figure 4.12.

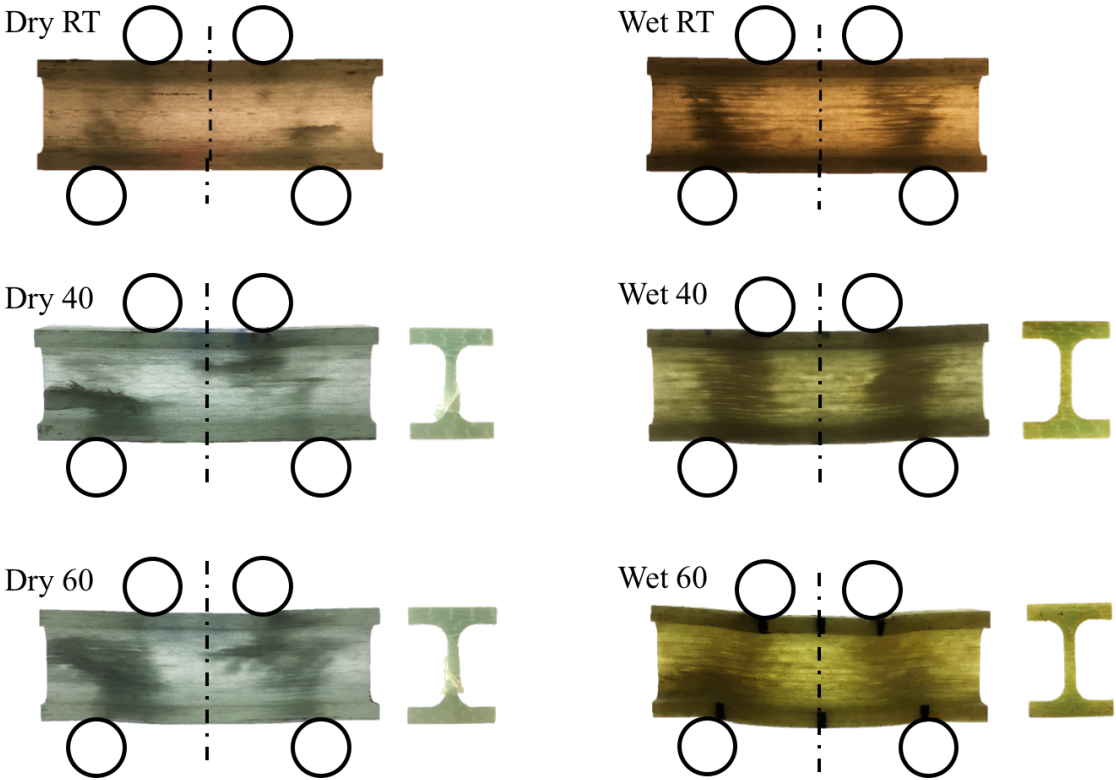


Figure 4.12: Light transmittance photos of specimens subsequent to fatigue testing.

The damage in the web was inspected using a confocal microscope (Alicona InfinteFocus 4G), and the results are presented in figure 4.13. It is seen that the dry sample at room temperature failed in the inter-ply, the resin rich area between the plies, while the dry samples tested at 40°C and 60°C failed in the intra-ply (in the ply). The wet samples tested at room temperature and 40°C both failed in the ply. It was difficult to obtain good quality images of the wet sample tested at 60°C. However, it looked like the sample failed by cracks that developed in both the inter-ply and the intra-ply, and the material looked rather destroyed. Numerous micro-cracks were observed over the whole length of the web in the wet samples, while the dry samples revealed one or two prominent cracks.

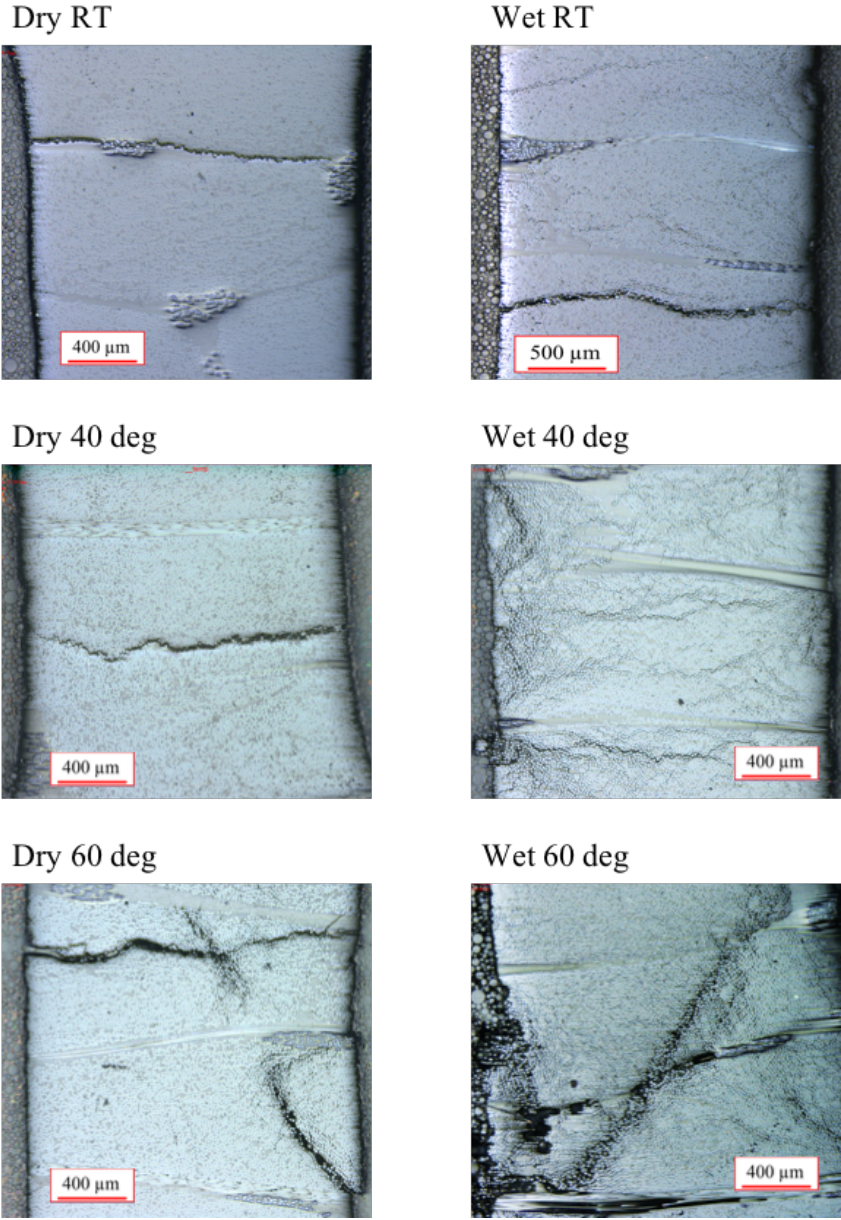


Figure 4.13: Microscopic observation of damage in the web of the beam's cross section for the different test environments.

#### 4.4.4 Deflection during fatigue testing

The maximum cyclic deflection is plotted against the normalized number of cycles in figure 4.14. All the curves follow a similar pattern with a significant initial slope, a constant, less steep, slope for the region in the middle and a gradual increase in slope towards the end of the lifetime. These regions are referred to as region I, II and III. This is observed as a typical behavior for composites [47]. The behavior of wet specimens tested at 60°C was an exception, and the reason for this is discussed in 5.5 and attributed to a lowering of the material's glass transition temperature,  $T_g$ , as a result of the conditioning. For the dry samples, the amount of the total lifetime a sample spent in stage III increased with increasing temperature. This is also the case for the wet samples. The same increase in the amount of the total lifetime spent in stage III was seen as a result of conditioning.

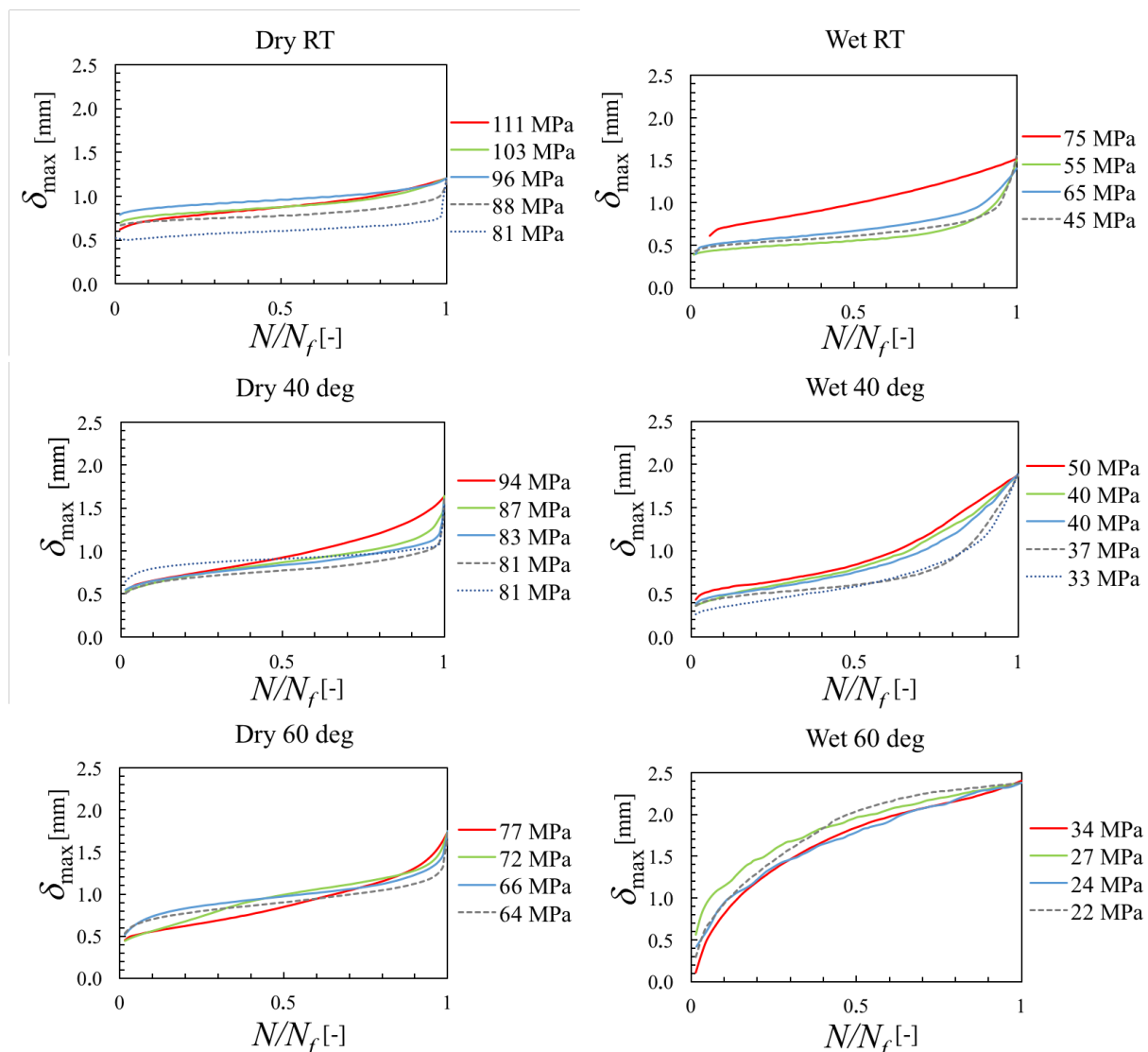


Figure 4.14: Maximum deflection versus the normalized number of cycles.

#### 4.4.5 Hysteresis loops, dissipated energy and stiffness evolution

Typical hysteresis loops for each test environment are presented in figure 4.15. One hysteresis loop corresponds to one load cycle. At what percentage of the total lifetime the load cycle took place is indicated by the legend. The amplitude and shape of the hysteresis loops depend on the applied load [41]. However, in order to compare the hysteresis loops of the different test environments, the author chose to compare samples failing at 20,000 – 60,000 cycles. As mentioned earlier, this equals a stress level in the area 62% to 65% of the ultimate shear strength ( $\tau_{max}$ ) for the dry samples and a stress level in the area 50% to 55% of the ultimate shear strength for the wet samples. The hysteresis loops originate from the same samples as seen in figure 4.12 and 4.13.

The area inside each hysteresis loop is proportional to the dissipated energy in each load cycle and referred to as the hysteresis dissipated energy (HDE) [41]. It is beneficial to calculate this value and plot it as in figure 4.16. As the HDE is dependent on the applied stress, it was normalized to the HDE in the first cycle to make comparison easier. For the dry samples, it was observed that the HDE experienced a limited increase until the very end of the samples' lifetime. The HDE at the end of the samples' lifetime increased with an increase in test temperature. The wet samples, on the other hand, showed a more gradual increase in HDE throughout the whole lifetime. This was true for all wet samples, except the one at 60°C.

The slope of the line between the maximum and the minimum shear stress in each hysteresis loop is called secant shear modulus. The secant shear modulus is beneficial to report, as it can be seen as a measurement of the amount of fatigue degradation. The evolution of secant shear modulus over the lifetime for each tested specimen is reported in figure 4.17. For both the dry and the wet samples, an increase in test temperature led to a drop in secant shear modulus at failure. This was more severe for the wet samples. All samples experienced a gradual decrease in secant shear modulus throughout the lifetime. This was, again, more severe for the wet samples than the dry ones.



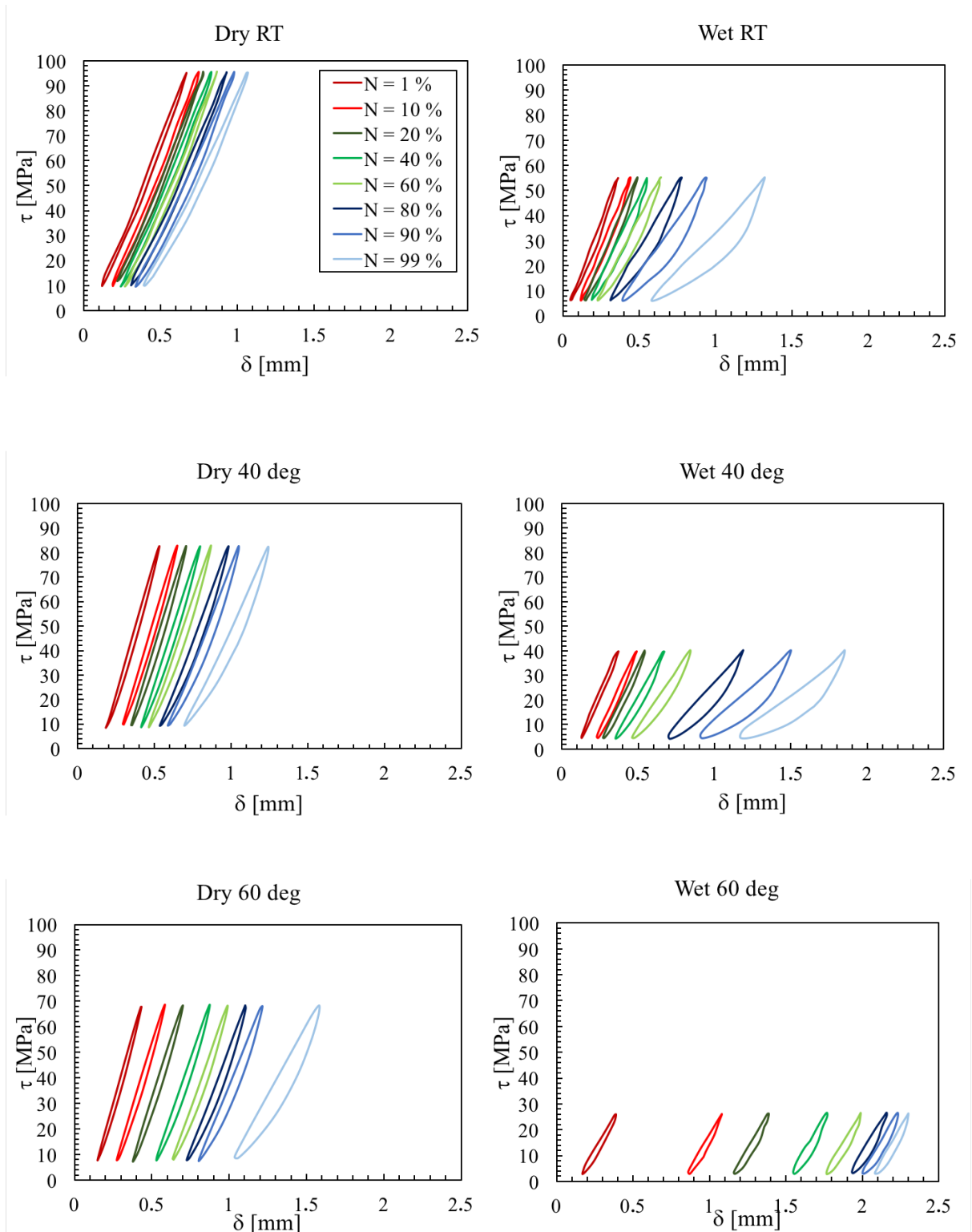


Figure 4.15: Representative hysteresis loops for each test environment.

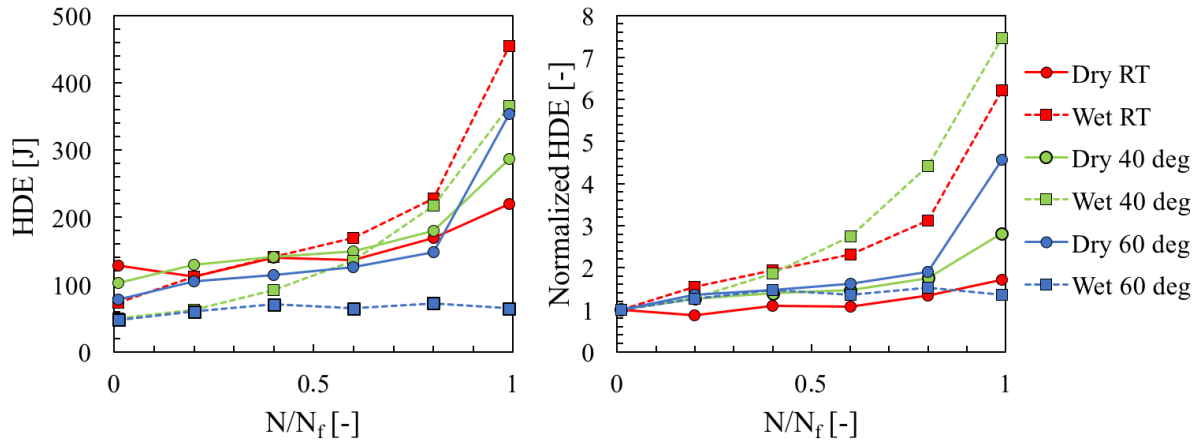


Figure 4.16: Fatigue evolution of absolute and normalized hysteresis dissipated energy (HDE).

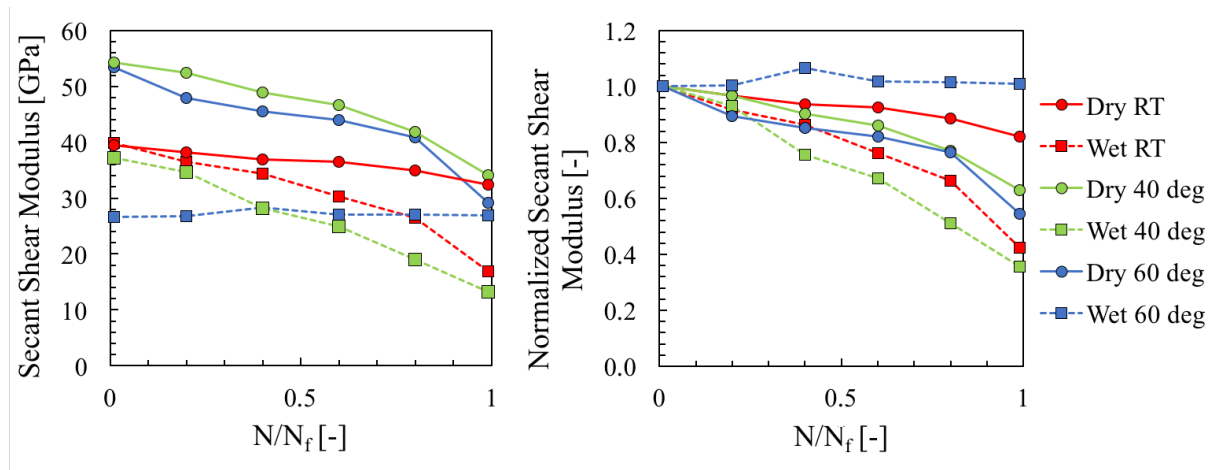


Figure 4.17: Fatigue evolution of absolute and normalized secant shear modulus.

## 5 Discussion

### 5.1 Discrepancy in water uptake

In figure 4.2, it is seen that the experimentally obtained mass uptake curve did not follow the analytical prediction curve exactly. Part of this discrepancy was expected, and explained in the following. In the section where the web meets the flange, the fillets result in diffusion lengths much higher than the diffusion lengths of the web and flange. The fillets were ignored in the analytic model, and the calculated saturation time of the beam was consequently underestimated. In addition, the flanges were modeled as fully submerged rectangular parallelepipeds, thus contributing to the underestimation.

In figure 4.2, it is also observed that the experimentally obtained mass uptake curve did not seem to flatten out as expected. As previously mentioned, the accuracy of modeling diffusion in composites with a Fickian approach is debated [18, 19]. At longer diffusion times, the weight gain of composites has shown to deviate from Fickian diffusion [48]. This has been attributed to changes in the epoxy network, i.e. creation of additional free volume, and debonding in the fiber/matrix interface. The debonding is caused by swelling and creates empty spaces in the composite that is subsequently filled with water, resulting in additional weight gain. This is most likely the reason for the additional and extreme mass uptake of the beams conditioned for a full year. The I-beam geometry is rather complex, and since the thickness of the web is smaller than the flange, it is assumed that the web reached saturation earlier than the flanges and fillets. As a result, parts of the I-beam experienced Fickian diffusion, while other parts experienced the "over-saturation" mechanisms mentioned above. It is speculated that this is the reason to why the mass uptake curve never seemed to flatten out. It should therefore be questioned if the analytical method is a good approach for predicting weight gain in the I-beam specimens.

It was seen that the experimental water uptake results were highly scattered, which means that each specimen absorbed water differently. Gagani et al. showed that water uptake is highly dependent on void volume, which might be the reason for the scattered results [23]. The void volume was not measured for the laminates used in this work. However, optical microscope analysis of the laminates indicated a very low void content.

## 5.2 Selecting the right fatigue failure limit

The definition of failure is an important factor to consider when performing fatigue tests. For tensile fatigue testing, the choice of failure limit is usually indisputable and chosen to be at the time when the specimen splits in two. For fatigue bending, on the other hand, the choice of failure limit is not as obvious since the tested specimen never will experience a complete partition. The fatigue data at room temperature was obtained by imposing a deflection limit equal to deflection at failure ( $\delta_f$ ) obtained by the static tests described in section 4.3.1. The author questioned this method, and tested every specimen to a deflection of 3 mm, i.e. the limitation of the test setup due to the anti-buckling device. A deflection of 3 mm is greater than any of the individual  $\delta_f$  values. In figure 5.1, the SN-curves corresponding to a failure limit of 3 mm are plotted alongside the SN-curves reported in the results (figure 4.11), which were obtained by imposing a failure limit equal  $\delta_f$  for each test environment. It is seen that choosing 3 mm as the deflection limit gives a negligible shift for the curves belonging to the dry samples. The shift is more prominent, but not dramatic, for the curves that belongs to the wet samples. The reason for this is the change of damage evolution as a result of conditioning. It will be discussed in detail later.

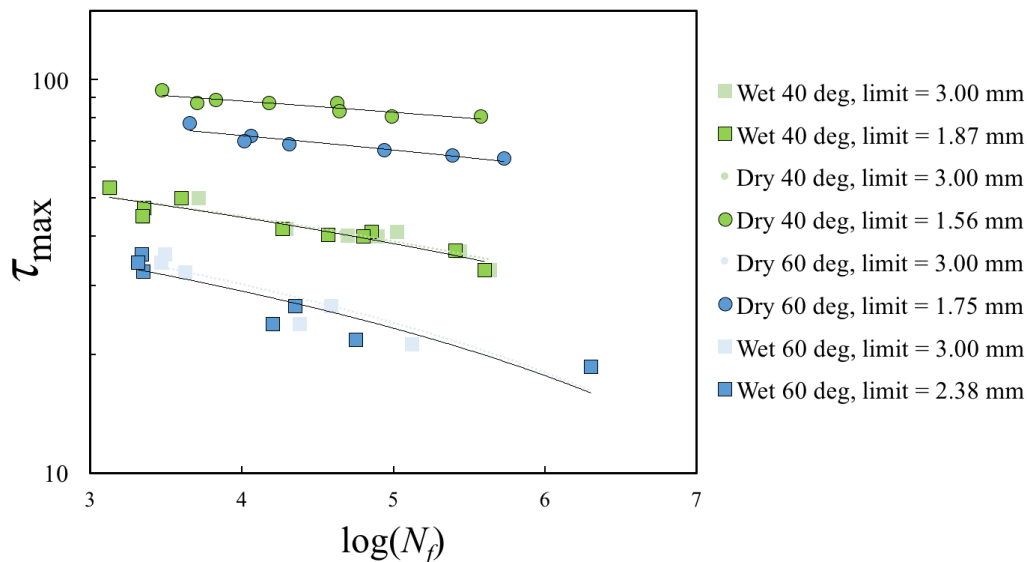


Figure 5.1: SN-curves with different fatigue failure deflection limits.

In the results section, the maximum deflection-cycle curves (see figure 4.14) for the fatigue tests were presented. It was pointed out that the majority of the curves followed the same pattern, with distinct regions referred to as region I, II and III. These regions are illustrated in figure 5.2. Region I is dominated by roller indentation and creation of

microcracks in the matrix [49, 1]. Region II is attributed to a slow crack growth where damage accumulates and eventually reach the fiber matrix interface [47]. The increase in maximum deflection in region II is also assumed to be attributed to creep. In region III, sufficient damage has accumulated for the cracks to grow rapidly. The transitioning from region II to region III can be chosen as the failure limit, as this is the point where the sample goes from being somewhat stable to unstable. By imposing this transition as the failure limit, still no dramatic change is observed for the SN-curves, as seen in figure 5.3. This indicates that the choice of failure limit has a very limited influence on the SN-curves for the material tested in this study.

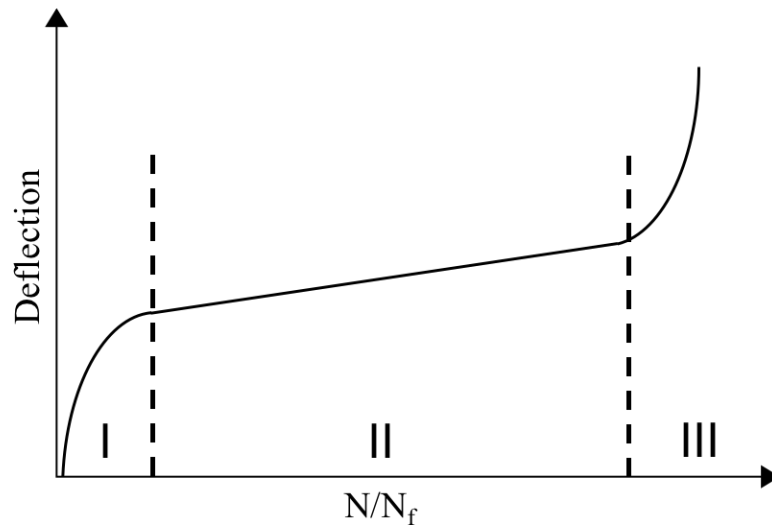


Figure 5.2: Schematic illustrating regions in fatigue testing, adapted from [1].

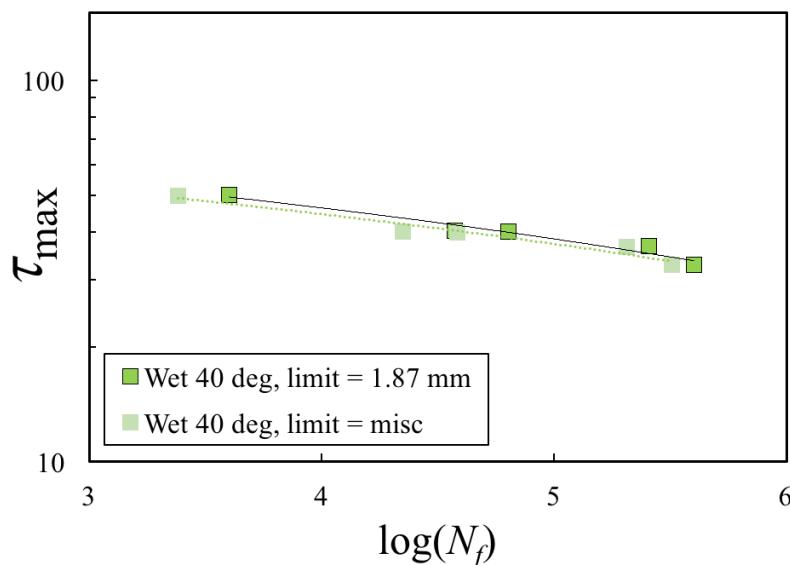


Figure 5.3: SN-curves with different fatigue failure limits.

### 5.3 Accuracy of test procedure

The experimentally obtained values for shear strength ( $\tau_{max}$ ) were three to four times higher than the strengths predicted by the micromechanical models developed by Chamis and Huang. It is speculated that the shear strength measured by the I-beam is tolerating some damage accumulation prior to what is defined as  $\tau_{max}$  in this work. Hence, the material is failing locally without it showing in the stress-deflection curve until a sufficient amount of damage is accumulated. Damage noises were heard during static testing for a while prior to a clear decay or drop in the stress-deflection curve, which supports this theory. It is believed that the shear strength values obtained by the micromechanical models represent shear stress values at which these local damages occur, rather than  $\tau_{max}$ . It is speculated that what is defined as yield strength in this work,  $\tau_Y$ , is a more representative shear stress value for where damage first occurs, as it coincides better with the analytical shear strength values than  $\tau_{max}$ . The defined yield strength in this work is therefore thought to be a result of both local material damage formation, i.e. matrix cracks and fiber-matrix debonding, and yielding of the matrix.

Rocha et al. measured both static and fatigue behavior of short beams with a square cross-section in a three-point bending configuration at room temperature [7]. They tested a material almost identical to the material tested in this work. They found a static shear strength in the area of 45 MPa and 30 MPa for dry and wet beams, respectively. These values are three to four times less than the values measured in this work and very similar to the values obtained by the micromechanical models of Chamis and Huang. It is therefore reasonable to believe that the square cross-sectional specimens represent a strength reflecting more on the material strength, while the I-beam specimens do not. This nature of damage accumulation in the I-beams makes it difficult to measure and define shear strength. The research group is currently trying to improve the understanding of the damage accumulation in the I-beams.

The experimentally obtained shear modulus strongly agrees with the analytically obtained shear moduli. However, these results should be treated with care due to the limitations, mentioned in 3.6.1, of the method used to obtain the values.

## 5.4 Temperature effects on dry specimens

An increase in test temperature led to an increase in deflection at failure, a decrease in shear strength and a decrease in yield stress measured by the static tests. This effect was more pronounced for the specimens tested at 60°C than 40°C. The mentioned properties are dominated by the matrix and/or interphase properties [3]. An increase in temperature leads to an increase in chain mobility in the matrix and the interphase. This effect increases rapidly as the temperature approaches the glass transition temperature ( $T_g$ ) of the material [6, 27, 50]. The increase in chain mobility in the matrix/interphase reduces the material's capacity to withstand loads. Hence, the ultimate shear strength, shear stiffness and yield stress are reduced. In addition, an increase in chain mobility results in a more ductile material behavior, and the deflection at failure increases as demonstrated in this study.

A composite's shear strength is affected by the properties of both the interphase and the matrix, while the shear modulus is only affected by the matrix properties [3]. The shear modulus increased by 1% for the specimens tested at 40°C compared to the tests performed at room temperature, which is considered a negligible effect. It decreased by 6% for the samples tested at 60°C compared to room temperature. The shear strength decreased by 8% and 24% for the samples tested at 40°C and 60°C, respectively, compared to room temperature. Hence, the shear strength was much more influenced by a temperature rise than the shear modulus. It is speculated that this indicates that the interphase is more influenced by a change in temperature than the matrix. It is shown in the literature that the  $T_g$  of the interphase is lower than the  $T_g$  of the matrix which supports this idea [51]. Failure and shear strength of composites, both experimentally and theoretically, are not fully understood yet due to their complex nature. More research is needed to confirm this hypothesis.

In this study, it was shown that the SN-curves shifted downwards with an increase in test temperature. The shift must be seen as a consequence of the reduced static shear strength. It is seen in figure 5.4 that the shear strength,  $\tau_{max}$ , followed  $\tau_0$  (fatigue regression parameter) with a change in temperature. The slope of the SN-curve increased when rising the test temperature from RT to 40°C, and then decreased slightly when rising the test temperature from 40°C to 60°C. An interesting observation found in this study was that the slope of the SN-curves tended to follow the static stiffness ( $G_{12}$ ) with a change in test temperature, see figure 5.5. Note that the stiffness of the dry specimens tested at RT reported in this graph was obtained by Gagani from laminate A, whereas the stiffness reported in the results section were obtained from laminate B. The reason for this is that

the specimens represented by the dry SN-curve at RT were made from laminate A, and thus a direct comparison can be made. Such a relation has never been pointed out in the literature to the author's knowledge. The author will not attempt to explain why these values seem to coincide. More research is needed to find out whether or not this relation is incidental.

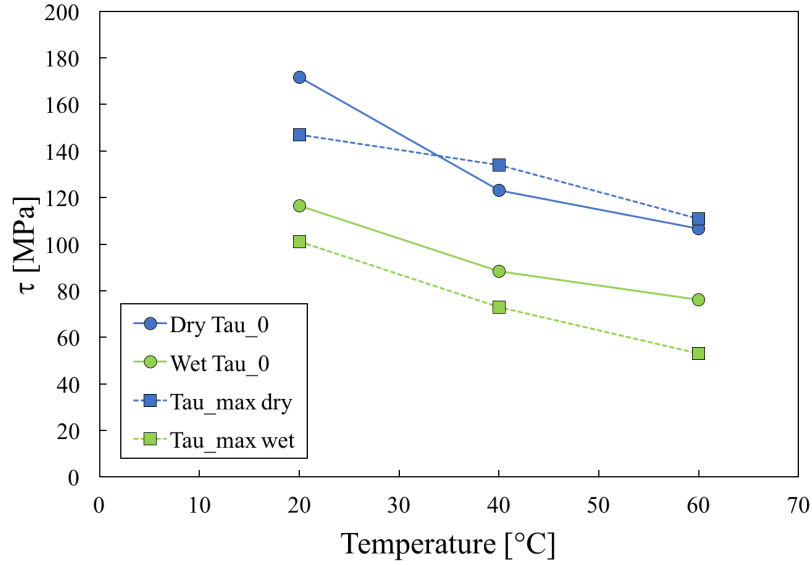


Figure 5.4: Comparison of static shear strength,  $\tau_{max}$ , and parameter from fatigue curve regression,  $\tau_0$ .

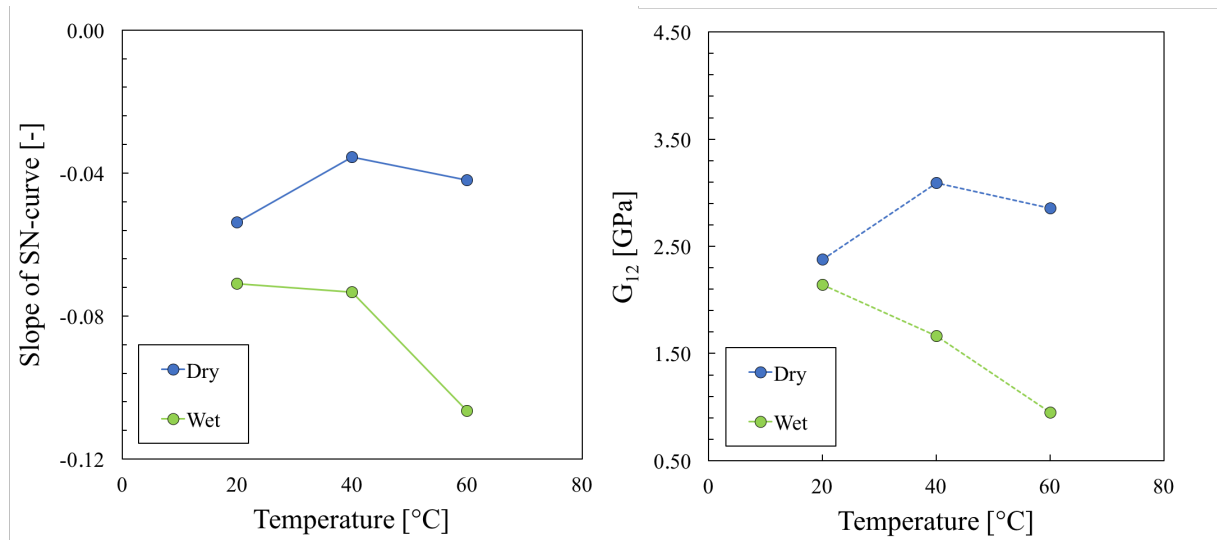


Figure 5.5: Comparison of static shear modulus,  $G_{12}$ , and slope of SN-curve,  $-1/k$ .

It was seen that for the specimens tested at room temperature, cracks appeared in the inter-ply region, while for the specimens tested at 40°C and at 60°C cracks appeared inside the ply (see figure 4.13). This might indicate that the interface between the fiber and matrix is more influenced by the temperature increase than the matrix for the material tested in this work. Consequently, the fiber/matrix interface becomes the weakest link in



the composite where cracks are initiated. It is speculated that this change of failure mode by an increasing test temperature is the reason for the change in slope of the SN-curves. More research is needed to find confirm this hypothesis.

It was observed that the hysteresis loops shifted to a greater extent with an increase in test temperature. A shift of the hysteresis loops indicates creep or damage in the material [41]. It is well known that creep effects increase in polymers with a rise in temperature. It was also seen a steady and limited increase in HDE and a limited decrease in secant shear modulus until the last 20% of the fatigue lifetime for the dry samples. This excludes that the shift of the hysteresis loops is caused by extensive damage in the material. Hence, the shift of hysteresis loops is mainly attributed to creep.

As mentioned earlier, the deflection curves can be divided into three regions, as illustrated in figure 5.2. For the dry samples, the amount of total fatigue lifetime spent in region III increased with an increase in test temperature. It was also observed that the samples dissipated more energy at the end of their lifetime with an increase in test temperature. Dissipation of energy can be seen as a result of damage and friction within cracks and delaminations [41]. It is believed that an increase in test temperature enabled more cracks to develop before the sample failed. The secant shear modulus at the end of the samples' lifetime decreased with an increase in test temperature. This suggests that more damage developed in region III at higher test temperatures, thus supporting this theory. The light transmittance photos and micrographs also support this theory, as they show larger damage areas and more cracks in the samples tested at higher temperatures. The deflection at failure increased with an increase in test temperature, indicating that the toughness increased [52]. When a crack was initiated in the material, the crack propagation rate was lowered due to the increase in toughness and, consequently, more cracks had the time to develop before the sample failed.

## 5.5 Temperature effects on wet specimens

As with the dry samples, the wet samples showed an increase in deflection at failure and a decrease in shear strength, yield stress and shear modulus as a result of a rise in test temperature. This is, again, attributed to the increased chain mobility with increasing temperature.

The SN-curves shifted downwards with a increased test temperature, and this downward shift followed the static shear strength as seen in figure 5.4. The slope of the SN-curves decreased with an increase in temperature. Upon writing this work, what is causing this

decrease in slope is unclear. More research is needed on the topic.

In this work, it was seen that the wet samples tested at 60°C exhibited a behavior dramatically different from all other samples tested in this work. When composites are immersed in water for a long period of time, the material's  $T_g$  gets severely reduced due to plasticizing [7]. The composite's  $T_g$  was measured by Gagani et al. to be 49°C after conditioning [53]. This is dramatically different than the  $T_g$  prior to conditioning (84, 7°C). Therefore, the tests performed at 60°C is conducted above  $T_g$  and the samples exhibit a somewhat rubbery behavior much different from the other samples in this work. Consequently, the results of wet samples tested at 60°C should be interpreted with caution and will not be discussed any further.

As with the dry samples, the toughness of the wet samples increased with an increase in test temperature. Consequently, the samples tested at 40°C spent a greater amount of its total fatigue life in region III (see figure 5.2) compared to the samples tested at RT. Hence, a larger number of cracks and delaminations had the time to develop before the sample failed. This is consistent with the increased HDE and decreased secant shear modulus for the samples tested at 40°C. The micrographs and light transmittance photos also indicate that a greater number of cracks developed in the samples tested at higher temperatures.

## 5.6 Effects of conditioning

By comparing the static results for the dry and wet samples, it is evident that conditioning and a rise in temperature shows analogous effects on the material. Conditioning leads to a reduction in shear strength, shear modulus and yield strength and an increase in deflection at failure. This is, again, attributed to an increase in chain mobility. As mentioned earlier, the increased chain mobility is caused by water molecules arranging themselves between the polymer chains, subsequently increasing the distance between them [25, 26]. Furthermore, conditioning leads to a downward shift of the SN-curves and a change in slope.

It is observed that the change of test temperature results in a more dramatic change in static properties for the wet samples compared to the dry ones. This is related to the lowering of the  $T_g$  as a result of the conditioning, and that the chain mobility increases rapidly as the temperature approaches the glass transition temperature [6, 27, 50].

Conditioning leads to a swelling of the matrix and interface, which potentially results in microcracking in the matrix and interface and/or fiber matrix debonding [18]. Fiber matrix debonding has been observed for the material tested in this study as a result of conditioning [10]. Consequently, cracks existed in the wet samples prior to fatigue testing, and these propagated during the fatigue life from the beginning of the test. This is consistent with the steady increase in HDE during the samples' lifetime. This is not observed for the dry samples, which suggest that cracks are not present in material from the beginning of the test. This has been confirmed by microscopy [10]. It is believed that the cracks that do eventually develop in the dry samples are creep initiated.

## 5.7 Application of results

As mentioned in the introduction, FRPs are often utilized in harsh environments. The FRP investigated in this work showed a severe degradation in both static and fatigue properties when exposed to water and heat. The wet samples tested at 60°C showed a 2/3 reduction in static shear strength compared to dry samples tested at room temperature. Hence, one should be cautious to utilize composites for components intended to survive 20 to 50 years or even longer in an offshore environment. The reason for the strength reduction, as a result of water ingress and/or a temperature increase, is the increased chain mobility in both the matrix and interface. Thus, for offshore components, one should consider using a matrix polymer whose chain mobility is less affected by water and heat. Another finding in this work was that all the samples tested in fatigue failed in the fiber matrix interface, thus the interface seemed to be the weakest link in the composite. Consequently, the results of this work might indicate that the interface (sizing) formulation should be changed or modified for composites intended for offshore environments. If it is not possible to improve the properties of the composite, it is necessary to design the composite component for highly reduced properties.

As claimed at the beginning of this report, long-term degradation of composites is not fully understood on a fundamental physical level. Thus, long-term prediction of composites' behavior is problematic. This results in tedious test programs in order to evaluate composite components for their respective applications. The test procedure presented in this work might contribute to reducing the mentioned test times. The saturation time is reduced as a result of the thin I-beam profile, and the four-point bending procedure enables to find material properties such as shear strength. However, as discussed in section 5.3, it seems that the I-beam geometry leads to an overestimation of the material properties compared to results found by Rocha et al. and micromechanical models [7].

It is worth noting that Rocha et al. measured a 1/3 static shear strength reduction of conditioned samples compared to dry samples. This is the same strength reduction measured at room temperature with the method presented in this work. Rocha et al. also showed that the SN-curve shifts downward in a similar way as is in this work, and that conditioned samples generated a steeper SN-curve compared to dry samples. Hence, it is believed that the method in this work can potentially, if not be applicable to obtain exact material properties, at least measure the relative change due to the presence of moisture in the material. More research is needed to confirm this hypothesis.

The fatigue data can potentially be fitted to a fatigue life estimation model. Such a model is presented by Mortazavian and Fatemi, which correlates fatigue data for different temperatures based on an Arrhenius equation curve fit [54]. If such a model is confirmed to work, and one can confidentially utilize it to predict fatigue behavior at different temperatures, test times will be dramatically reduced.

## 6 Conclusions

In this master thesis, the influence of environmental effects on glass fiber/epoxy composites' static and fatigue behavior was studied. This was accomplished by performing a four-point bending test procedure of dry and conditioned I-beam specimens at different test temperatures. The key findings can be summarized as follows;

- The samples did not seem to saturate completely and did not follow a Fickian diffusion. Four samples were still absorbing water after a full year of conditioning.
- A rise in test temperature leads to a decrease in shear strength, shear modulus and yield strength and an increase in deflection at failure. These effects are more severe for conditioned samples.
- There is an analogous effect of heat and water on static properties, both soften the material and lead to a decrease in shear strength, shear modulus and yield strength and an increase in deflection at failure.
- A rise in temperature shifts the SN-curves downwards. The downward shift is more severe for the SN-curves belonging to the conditioned samples. A change of test temperature leads to changes in the slope of the SN-curves, and this seem to follow the changes in shear modulus.
- There is an analogous effect of heat and water on fatigue behavior, both lead to a downward shift of the SN-curves and a change of slope.
- Conditioning leads to a change in failure mode. Fatigue cracks are creep-initiated for the dry samples, while swelling-induced for the wet samples.

These findings help to increase the understanding of long-term behaviour in composites (fiber reinforced polymers).

### **Further work**

The work presented in this thesis is part of a bigger project that aims to develop mathematical models intended to predict long-term behavior of composites. The research group is currently working on improving or developing the different parts of the multiscale model mentioned in section 2.3. A great amount research remains to be done before reaching a satisfactory and functioning multiscale model. Further work linked to this thesis, in-

cludes to try to implement the data obtained in this study in models like Mortazavian and Fatemis' fatigue life estimation model [54]. It might be necessary to perform additional tests at various temperatures to increase the amount of input data for the mentioned model. Additional tests should also be performed to increase the confidence in the data obtained by the short-beam bending procedure described in this thesis, and thus potentially detect the reason for the overestimation of beams' shear strength. Furthermore, why the I-beams do not follow a Fickian diffusion should be investigated.

## 7 References

- [1] A. Varvani-Farahani and A. Shirazi, “A fatigue damage model for (0/90) frp composites based on stiffness degradation of 0 and 90 composite plies,” *Journal of Reinforced Plastics and Composites*, vol. 26, no. 13, pp. 1319–1336, 2007.
- [2] A. T. Echtermeyer, T. S. Ekeberg, and O. E. Sund, “Long-term testing of composite through-thickness properties,” Health and Safety Executive, HSE, United Kingdom, Tech. Rep., 2004.
- [3] B. D. Agarwal, L. J. Broutman, and K. Chandrashekhara, *Analysis and performance of fiber composites*. John Wiley & Sons, 2017.
- [4] Z.-M. Huang and Y.-X. Zhou, *Strength of fibrous composites*. Springer Science & Business Media, 2012.
- [5] E. P. Sideridis and G. S. Bikakis, “Shear properties and load–deflection response of cross–ply glass–epoxy composite short–beams subjected to three–point–bending tests, and the effect of moisture absorption,” *Journal of Applied Polymer Science*, vol. 129, no. 4, pp. 2244–2252, 2013.
- [6] Z. Ullah, S. Grammatikos, M. Evernden, C. Pearce *et al.*, “Multi-scale computational homogenisation to predict the long-term durability of composite structures,” *Computers & Structures*, vol. 181, pp. 21–31, 2017.
- [7] I. Rocha, S. Rajjmaekers, R. Nijssen, F. van der Meer, and L. Sluys, “Hygrothermal ageing behaviour of a glass/epoxy composite used in wind turbine blades,” *Composite Structures*, vol. 174, pp. 110–122, 2017.
- [8] A. T. Echtermeyer, A. Gagani, A. Krauklis, and T. Mazan, “Multiscale modelling of environmental degradation—first steps,” in *Durability of Composites in a Marine Environment 2*. Springer, 2018, pp. 135–149.
- [9] “Standard test method for short-beam strength of polymer matrix composite materials and their laminates, ASTM D2344 Standard,” American Society for Testing and Materials (ASTM), Tech. Rep., 1965.

- [10] A. Gagani, E. Mialon, and A. Echtermeyer, “Influence of hygrothermal ageing on interlaminar fatigue strength of gf/epoxy i-beams.” *Manuscript submitted for publication*, 2018.
- [11] K. K. Chawla, *Composite materials: science and engineering*. Springer Science & Business Media, 2012.
- [12] A. Shaw, S. Sriramula, P. D. Gosling, and M. K. Chryssanthopoulos, “A critical reliability evaluation of fibre reinforced composite materials based on probabilistic micro and macro-mechanical analysis,” *Composites Part B: Engineering*, vol. 41, no. 6, pp. 446–453, 2010.
- [13] M. Hinton and P. Soden, “Predicting failure in composite laminates: the background to the exercise,” *Composites Science and Technology*, vol. 58, no. 7, pp. 1001–1010, 1998.
- [14] P. Soden, A. Kaddour, and M. Hinton, “Recommendations for designers and researchers resulting from the world-wide failure exercise,” *Composites Science and Technology*, vol. 64, no. 3, pp. 589–604, 2004.
- [15] C. C. Chamis, “Simplified composite micromechanics equations for strength, fracture toughness, impact resistance and environmental effects.” NASA Lewis Research Center, Tech. Rep., 1984.
- [16] P. L. Murthy and C. C. Chamis, “Integrated composite analyzer (ican)-users and programmers manual.” NASA Lewis Research Center, Tech. Rep., 1986.
- [17] Z.-M. Huang, “Micromechanical prediction of ultimate strength of transversely isotropic fibrous composites,” *International Journal of Solids and Structures*, vol. 38, no. 22, pp. 4147–4172, 2001.
- [18] C. L. Schutte, “Environmental durability of glass-fiber composites,” *Materials Science and Engineering: R: Reports*, vol. 13, no. 7, pp. 265–323, 1994.
- [19] Y. Hu, A. W. Lang, X. Li, and S. R. Nutt, “Hygrothermal aging effects on fatigue of glass fiber/polydicyclopentadiene composites,” *Polymer Degradation and Stability*, vol. 110, pp. 464–472, 2014.
- [20] W. Jost, *Diffusion in solids, liquids, gases*. Academic press, 1952.
- [21] J. Crank, *The mathematics of diffusion*. Oxford university press, 1979.



- [22] M. Blikstad, P. O. Sjöblom, and T. R. Johannesson, “Long-term moisture absorption in graphite/epoxy angle-ply laminates,” *Journal of Composite Materials*, vol. 18, no. 1, pp. 32–46, 1984.
- [23] A. Gagani, Y. Fan, A. H. Muliana, and A. T. Echtermeyer, “Micromechanical modeling of anisotropic water diffusion in glass fiber epoxy reinforced composites,” *Journal of Composite Materials*, 2017.
- [24] I. B. C. M. Rocha, F. P. van der Meer, R. P. L. Nijssen, and L. J. Sluys, “A multiscale and multiphysics numerical framework for modelling of hygrothermal ageing in laminated composites,” *International Journal for Numerical Methods in Engineering*, vol. 112, no. 4, pp. 360–379, 2017.
- [25] K. Thomson, T. Wong, and L. Broutman, “The plasticization of an epoxy resin by dibutylphthalate and water,” *Polymer Engineering & Science*, vol. 24, no. 16, pp. 1270–1276, 1984.
- [26] B. Abdel-Magid, S. Ziaee, K. Gass, and M. Schneider, “The combined effects of load, moisture and temperature on the properties of e-glass/epoxy composites,” *Composite Structures*, vol. 71, no. 3, pp. 320–326, 2005.
- [27] J. W. Gooch, Ed., *Encyclopedic Dictionary of Polymers*. Springer New York, 2007.
- [28] E. Vauthier, J. Abry, T. Bailliez, and A. Chateauminois, “Interactions between hygrothermal ageing and fatigue damage in unidirectional glass/epoxy composites,” *Composites Science and Technology*, vol. 58, no. 5, pp. 687–692, 1998.
- [29] J. Thomason, L. Yang, and R. Meier, “The properties of glass fibres after conditioning at composite recycling temperatures,” *Composites Part A: Applied Science and Manufacturing*, vol. 61, pp. 201–208, 2014.
- [30] D. Hartman, M. E. Greenwood, and D. M. Miller, “High strength glass fibers,” *Moving Forward With 50 Years of Leadership in Advanced Materials.*, vol. 39, pp. 521–533, 1994.
- [31] O. Basquin, “The exponential law of endurance tests,” in *American Society for Testing and Materials Proceedings*, vol. 10, 1910, pp. 625–630.
- [32] A. Malpot, F. Touchard, and S. Bergamo, “Influence of moisture on the fatigue behaviour of a woven thermoplastic composite used for automotive application,” *Materials & Design*, vol. 98, pp. 12–19, 2016.

- [33] “HiPer-tex™ W2020 Rovings, Technical Datasheet,” 3B, Tech. Rep., 2011.
- [34] “EPIKOTE™ Resin MGS™ RIMR 135 and EPIKURE™ Curing Agent MGS™ RIMH 134–RIMH 137, Technical Datasheet,” Momentive, Tech. Rep., 2006.
- [35] C. Næss, “Master Thesis: Long-term properties of the matrix of composites,” *Norwegian University of Science and Technology, NTNU*, 2016.
- [36] “Standard test method for moisture absorption properties and equilibrium conditioning of polymer matrix composite materials, ASTM D5299 Standard,” American Society for Testing and Materials (ASTM), Tech. Rep., 1992.
- [37] “Standard test methods for fiber content of resin-matrix composites by matrix digestion, ASTM D3171 Standard,” American Society for Testing and Materials (ASTM), Tech. Rep., 1982.
- [38] “Standard test method for flexural properties of sandwich constructions, ASTM C393 Standard,” American Society for Testing and Materials (ASTM), Tech. Rep., 2000.
- [39] D. Jourawski, “Sur la résistance d’un corps prismatique et d’une pièce composée en bois ou en tôle de fer à une force perpendiculaire à leur longueur,” in *Annales des Ponts et Chaussées*, vol. 12, 1856, pp. 328–351.
- [40] J. Dally and L. Broutman, “Frequency effects on the fatigue of glass reinforced plastics,” *Journal of Composite Materials*, vol. 1, no. 4, pp. 424–442, 1967.
- [41] A. V. Movahedi-Rad, T. Keller, and A. P. Vassilopoulos, “Fatigue damage in angle-ply gfrp laminates under tension-tension fatigue,” *International Journal of Fatigue*, 2017.
- [42] G. S. Springer, *Environmental effects on composite materials. Volume 3*. Technomic Publishing Co., Inc., Lancaster, PA, 1988.
- [43] A. E. Krauklis, “Hygrothermal aging of fiber-reinforced composites: Introduction to phenomenological perspective and mass balance approach,” *Planned to be presented on 21st International Conference on Composite Structures (ICCS21)*, 2018.
- [44] A. E. Krauklis, “Hygrothermal aging of amine epoxy: Reversible static and fatigue properties,” *Manuscript submitted for publication*, 2018.
- [45] G. Lubin, *Handbook of composites*. Springer Science & Business Media, 2013.

- [46] P. Soden, M. Hinton, and A. Kaddour, “Lamina properties, lay-up configurations and loading conditions for a range of fibre reinforced composite laminates,” in *Failure Criteria in Fibre-Reinforced-Polymer Composites*. Elsevier, 2004, pp. 30–51.
- [47] D. S. de Vasconcellos, F. Touchard, and L. Chocinski-Arnault, “Tension–tension fatigue behaviour of woven hemp fibre reinforced epoxy composite: a multi-instrumented damage analysis,” *International Journal of Fatigue*, vol. 59, pp. 159–169, 2014.
- [48] A. Chateauminois, L. Vincent, B. Chabert, and J. Soulier, “Study of the interfacial degradation of a glass-epoxy composite during hygrothermal ageing using water diffusion measurements and dynamic mechanical thermal analysis,” *Polymer*, vol. 35, no. 22, pp. 4766–4774, 1994.
- [49] H. G. Kotik and J. E. P. Ipiña, “Short-beam shear fatigue behavior of fiber metal laminate (glare),” *International Journal of Fatigue*, vol. 95, pp. 236–242, 2017.
- [50] A. Tcharkhtchi, S. Faivre, L. Roy, J. Trotignon, and J. Verdu, “Mechanical properties of thermosets,” *Journal of materials science*, vol. 31, no. 10, pp. 2687–2692, 1996.
- [51] Y. Joliff, L. Belec, and J. Chailan, “Modified water diffusion kinetics in an unidirectional glass/fibre composite due to the interphase area: Experimental, analytical and numerical approach,” *Composite Structures*, vol. 97, pp. 296–303, 2013.
- [52] V. Gupta, L. Drzal, C.-C. Lee, and M. Rich, “The temperature-dependence of some mechanical properties of a cured epoxy resin system,” *Polymer Engineering & Science*, vol. 25, no. 13, pp. 812–823, 1985.
- [53] A. Gagani, A. Krauklis, N. Vedvik, and A. Echtermeyer, “Experimental study of interlaminar shear strength of glass fiber epoxy composites in humid environments. methodology and results.” *Manuscript submitted for publication*, 2018.
- [54] S. Mortazavian and A. Fatemi, “Fatigue behavior and modeling of short fiber reinforced polymer composites including anisotropy and temperature effects,” *International Journal of Fatigue*, vol. 77, pp. 12 – 27, 2015.



## 8 Appendix

### (A) Task description

NTNU - NORWEGIAN UNIVERSITY  
OF SCIENCE AND TECHNOLOGY  
DEPARTMENT OF MECHANICAL  
AND INDUSTRIAL ENGINEERING

**MASTER THESIS FALL 2017  
FOR  
STUD. TECHN. ANNA MONSÅS**

**Long-Term Properties of Interlaminar Shear Strength of Composite Laminates**

Composite laminates are widely used in demanding applications. Understanding the long-term performance is essential for using composites in components with lifetimes of 20 to 50 years or even longer. This thesis is part of a larger project investigating the long-term performance of composites in different environments. The thesis work will focus on measuring fatigue lifetime curves (SN curves) of the interlaminar strength at different temperatures. The SN curves will be measured in bending using novel test specimens having an I-beam shape. The temperature dependence shall be analysed and methods to predict long-term performance shall be explored.

## (B) Data from static tests

Table 8.1: Data from static tests executed in this work.

Environment	Ultimate load [kN]	$\tau_{max}$ [MPa]	$\tau_Y$ [MPa]	$G_{12}$ [GPa]	$\delta_f$ [mm]
Dry RT	9.25	142	72	3.04	1.49
	10.17	156	77	3.17	1.78
	9.42	145	79	2.99	1.74
	9.13	140	66	3.02	1.49
Mean values	9.49	146	74	3.05	1.63
Dry 40 deg	8.76	134	73	3.06	1.48
	8.73	134	71	3.10	1.66
	8.67	133	76	3.11	1.73
	8.84	136	74	3.10	1.68
Mean values	8.75	134	73	3.09	1.64
Wet 40 deg	5.08	78	42	1.63	1.95
	4.74	73	41	1.82	1.90
	4.76	73	43	1.99	1.68
	4.50	69	39	1.77	1.96
Mean values	4.77	73	41	1.80	1.87
Dry 60 deg	7.73	119	68	2.99	1.89
	7.27	112	66	3.00	1.69
	6.60	101	62	2.73	1.67
	-	-	63	2.81	-
Mean values	7.20	111	65	2.88	1.75
Wet 60 deg	3.62	55	25	1.17	2.37
	3.54	54	23	1.05	2.07
	3.24	50	20	0.75	2.71
	-	-	22	0.51	-
Mean values	3.47	53	22	0.87	2.38

## (C) Data from fatigue tests

Table 8.2: Fatigue life and testing conditions of the dry specimens.

Temperature	$\tau_{max}$ [MPa]	R-ratio	$N_f$
40 deg	94	0.10	2,981
	89	0.10	6,727
	87	0.10	5,046
	87	0.10	42,355
	87	0.10	15,175
	83	0.10	44,200
	81	0.10	98,000
	81	0.10	378,800
	74	0.10	2,000,000 (runout)
	61	0.10	2,000,000 (runout)
60 deg	77	0.10	4,500
	72	0.10	11,526
	70	0.10	10,371
	69	0.10	20,625
	66	0.10	87,000
	64	0.10	245,940
	63	0.10	534,522
61	0.10	2,000,000 (runout)	

Table 8.3: Fatigue life and testing conditions of the wet specimens.

Temperature	$\tau_{max}$ [MPa]	R-ratio	$N_f$	Days of conditioning
40 deg	53	0.15	1,343	101
	50	0.10	4,000	133
	47	0.12	2,261	101
	45	0.10	2,211	101
	42	0.10	18,458	106
	41	0.23	71,336	112
	40	0.11	37,236	115
	40	0.11	63,568	116
	37	0.10	256,856	116
	33	0.11	400,840	117
60 deg	36	0.26	2,195	108
	34	0.25	2,060	119
	32	0.11	2,247	108
	27	0.10	22,496	119
	24	0.10	16,028	120
	22	0.10	56,336	133
	19	0.10	2,000,000	120



(D) Light transmittance photos

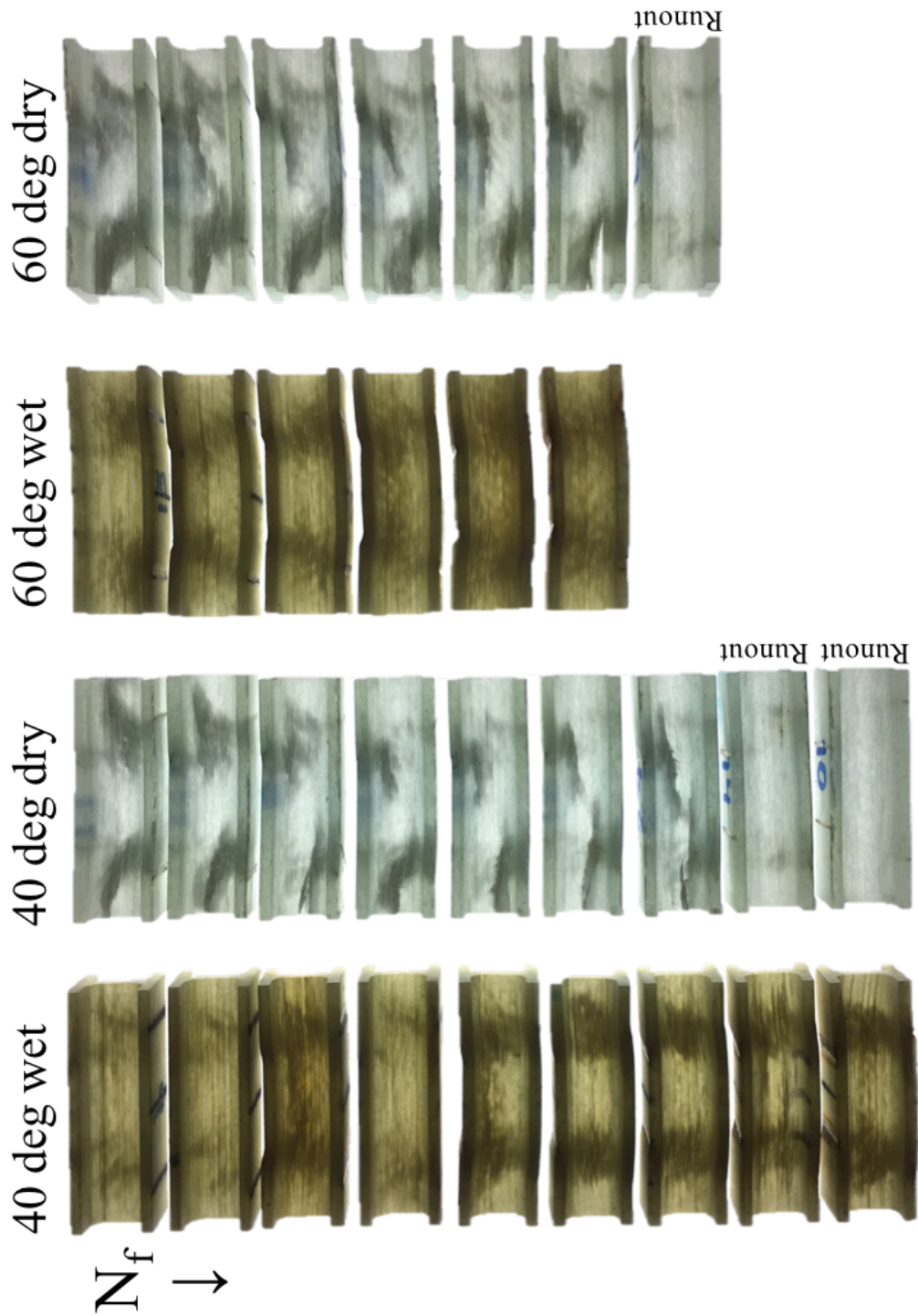


Figure 8.1: Light transmittance photos of every specimen tested in fatigue.

**(E) Risk assessment**

NTNU		Kartlegging av risikofylt aktivitet		Utarbeidet av		Nummer		Dato	
				HMS-avd.		HMSRV2601		22.03.2011	
HMS				Godkjent av				Erslatter	
				Rektor				01.12.2006	

## Kartlegging av risikofylt aktivitet

Enhet: MTP

Linjeleder: Torgeir Welo

Deltakere ved kartleggingen (m/ funksjon): Student Anna Monsås, VEILEDER ANDREAS ECHTERMEYER  
 (Ansv. veileder, student, evt. medveiledere, evt. andre m. kompetanse)

Kort beskrivelse av hovedaktivitet/hovedprosess: Masteroppgave av student Anna Monsås. Tittel på oppgaven er ikke satt enda.

Er oppgaven rent teoretisk? (JA/NEI): NEI

«JA» betyr at veileder inntar for at oppgaven ikke inneholder noen aktiviteter som krever risikovurdering. Dersom «JA»: Beskriv kort aktiviteten i kartleggingskjemaet under. Risikovurdering trenger ikke å fylles ut.

Signaturer: Ansvarlig veileder: 

Student: Anna B. Monsås

Dato: 12.09.17

ID nr.	Aktivitet/prosess	Ansvarlig	Eksisterende dokumentasjon	Eksisterende sikringstiltak	Lov, forskrift o.l.	Kommentar
1	Kutte til prøvestykker fra komposittplate	NN	Intern prosedyre for bruk av diamantsag.	Godkjent utstyr (diamantsag) og bruk av verneutstyr.	HMS - NTNU	
2	Maskinering av prøvestykker	NN	Intern prosedyre for bruk av fres.	Godkjent fresemasking og bruk av vernebriller.	HMS - NTNU	
3	Testing av prøvestykker	NN	Intern prosedyre for bruk av strekkestemaskiner	Godkjent maskiner og bruk av vernebriller	HMS - NTNU	
4	Produksjon av komposittplate	NN	Intern prosedyre for bruk av komposittflab	Bruk av verneutstyr	HMS - NTNU	

NTNU		Risikovurdering		Dato	
HMS				22.03.2011	
				Erstatter	
				01.12.2006	
Utarbeidet av		Nummer			
HMS-avd.		HMSRV2601			
Godkjent av					
Rektor					

Enhet: MTP

Linjeleder: Torgeir Welo

Deltakere ved kartleggingen (m/ funksjon): Student Anna Monsås , VEILEDER ANDREAS ECHTERMEYER  
 (Ansv. Veileder, student, evt. medveiledere, evt. andre m. kompetanse)

Risikovurderingen gjelder hovedaktivitet: Masteroppgave student Anna Monsås. Tittel på oppgaven er ikke satt enda.

Signaturer: Ansv. veileder:  Student: Anna B. Monsås

Dato: 12.09.17

ID nr	Aktivitet fra kartleggings-skjemaet	Mulig uønsket hendelse/belastning	Vurdering av sannsynlighet (1-5)	Vurdering av konsekvens:				Risiko-Verdi (menneske)	Kommentarer/status Forslag til tiltak
				Menneske (A-E)	Ytre miljø (A-E)	ØK/ materiell (A-E)	Om-dørme (A-E)		
1	Kutte til prøvestykker fra komposittplate	Kuttskader	1	B	A	A	A	B1	Hold alltid en hånd på håndtaket når bladet roterer
1		Flyvende prøvestykker grunnet mye friksjon fra bladet	2	A	A	A	A	A2	Prøve å feste eller holde prøvestykket godt fast
1		Kuttestøv på øyne, i innånding og på tøy	2	A	A	A	A	A2	Bruk av vernebriller, maske og labfrakk
2	Maskinering av prøvestykker	Løse gjenstander, hår, klesplagg o.l. blir dratt inn i de roterende delene av fresen	1	B	A	A	A	B1	Redusere antall mulige gjenstander som kan bli dratt inn i de roterende delene; langt hår (bør settes opp), smykker, skjorter med lange ermer osv
2		Maskineringsspon på øyne	1	B	A	A	A	B1	Forsøke å styre sponet i motsatt retning av operatøren, bruk vernebriller
2		Kuttskader	1	B	A	A	A	B1	Unngå å berøre spon eller verktøy når fresen roterer



NTNU	<b>Risikovurdering</b>			Utarbeidet av	Nummer	Dato
				HMS-avd.	HMSRV2601	22.03.2011
HMS				Godkjent av		Erstatter
		Rektor		01.12.2006		



### Sannsynlighet vurderes etter følgende kriterier:

Svært liten 1	Liten 2	Middels 3	Stor 4	Svært stor 5
1 gang pr 50 år eller sjeldnere	1 gang pr 10 år eller sjeldnere	1 gang pr år eller sjeldnere	1 gang pr måned eller sjeldnere	Skjer ukentlig

### Konsekvens vurderes etter følgende kriterier:


Gradering	Menneske	Ytre miljø Vann, jord og luft	Øk/materiell	Omdømme
<b>E</b> Svært Alvorlig	Død	Svært langvarig og ikke reversibel skade	Drifts- eller aktivitetstans > 1 år.	Troverdighet og respekt betydelig og varig svekket
<b>D</b> Alvorlig	Alvorlig personskade. Mulig uførhet.	Langvarig skade. Lang resitusjonstid	Driftstans > ½ år Aktivitetstans i opp til 1 år	Troverdighet og respekt betydelig svekket
<b>C</b> Moderat	Alvorlig personskade.	Mindre skade og lang resitusjonstid	Drifts- eller aktivitetstans < 1 mnd	Troverdighet og respekt svekket
<b>B</b> Liten	Skade som krever medisinsk behandling	Mindre skade og kort resitusjonstid	Drifts- eller aktivitetstans < 1 uke	Negativ påvirkning på troverdighet og respekt
<b>A</b> Svært liten	Skade som krever førstehjelp	Ubetydelig skade og kort resitusjonstid	Drifts- eller aktivitetstans < 1 dag	Liten påvirkning på troverdighet og respekt

### Risikoverdi = Sannsynlighet x Konsekvens

Beregn risikoverdi for Menneske. Enheten vurderer selv om de i tillegg vil beregne risikoverdi for Ytre miljø, Økonomi/materiell og Omdømme. I så fall beregnes disse hver for seg.

### Til kolonnen "Kommentarer/status, forslag til forebyggende og korrigerende tiltak":

Tiltak kan påvirke både sannsynlighet og konsekvens. Prioriter tiltak som kan forhindre at hendelsen inntreffer, dvs. sannsynlighetsreduserende tiltak foran skjerpet beredskap, dvs. konsekvensreduserende tiltak.

NTNU		Risikomatrix		Dato	
				08.03.2010	
HMS/IKS				Erstatter	
		utarbeidet av		Nummer	
		HMS-avd.		HMSRV2604	
		godkjent av			
		Rektor		09.02.2010	



## MATRISSE FOR RISIKOVURDERINGER ved NTNU

KONSEKVENSENS		E1	E2	E3	E4	E5
		D1	D2	D3	D4	D5
Svært alvorlig		C1	C2	C3	C4	C5
Alvorlig		B1	B2	B3	B4	B5
Moderat		A1	A2	A3	A4	A5
Liten		Svært liten	Liten	Middels	Stor	Svært stor
Svært liten		SANNSYNLIGHET				

Prinsipp over akseptkriterium. Forklaring av fargene som er brukt i risikomatrixen.

Farge	Beskrivelse
Rød	Uakseptabel risiko. Tiltak skal gjennomføres for å redusere risikoen.
Gul	Vurderingsområde. Tiltak skal vurderes.
Grønn	Akseptabel risiko. Tiltak kan vurderes ut fra andre hensyn.